

# **GEOLOGY FOR SOCIETY**

SINCE 1858



**GEOLOGICAL  
SURVEY OF  
NORWAY**

· NGU ·

# **NGU REPORT 2025.013**

---

Deep geothermal potential of Møre &  
Romsdal



GEOLOGICAL  
SURVEY OF  
NORWAY  
- NGU -

# NGU REPORT

Geology for society

Geological Survey of Norway  
P.O. Box 6315 Torgarden  
NO-7491 Trondheim, Norway  
Tel. +47 73 90 40 00

**Report no.:** 2025.013  
**ISSN:** 0800-3416 (print)  
**ISSN:** 2387-35150 (digital)  
**Grading:** Open

**Title:** Deep geothermal potential of Møre & Romsdal  
**Authors:** Yuriy Maystrenko  
**Client:** NGU  
**County:** Møre og Romsdal  
**Municipality:** Molde

**Map-sheet name (M=1:250.000):**  
**Map-sheet name (M=1:50.000):**  
**Deposit name and grid-reference:** WGS84 UTM32N 250000E, 550000E, 6850000N, 7100000N  
**Numbers of pages:** 36  
**Price (NOK):**

**Map enclosures:**  
**Fieldwork carried out:**  
**Date of report:** April 8<sup>th</sup> 2025  
**Project no.:** 401000  
**Person responsible:** Marco Brønner  
**Keywords:** 3D thermal modelling, temperature logs, geothermal energy, subsurface temperature

## Summary:

This study presents an evaluation of the deep geothermal energy potential of Møre & Romsdal County based on an integrated analysis of geological, geophysical, and thermal datasets. The research integrates borehole temperature logs, laboratory-measured rock properties, heat flow density estimates, and regional tectonic features to perform a 3D thermal modelling. The results indicate that temperatures increase from inland areas toward the coast and offshore regions, where sedimentary insulation enhances the geothermal gradient.

Key controlling factors include lithospheric thickness, crustal radiogenic heat production, groundwater flow dynamics, and the insulating effect of low-conductivity sediments. Offshore areas exhibit the highest geothermal potential, with temperatures at 5 km depth reaching ~150°C, sufficient for electricity generation. In contrast, mainland temperatures at similar depths remain lower (~124°C at 5 km), making them more suitable for direct heat applications rather than power production. The study also identifies structural complexities as a critical issue for accurate thermal modelling.

The results support the possibility of deep geothermal energy as a sustainable alternative to fossil fuels, particularly near coastal urban areas and offshore hydrocarbon platforms. Future work should refine the 3D thermal model with higher-resolution data and assess fluid flow dynamics to optimize geothermal resources assessment. This research contributes to regional and national energy strategies, supporting Norway's transition toward renewable energy with future reducing greenhouse gas emissions.

## Table of contents

1. INTRODUCTION.....	5
2. LARGE-SCALE GEOTHERMAL OVERVIEW .....	5
3. Subsurface Thermal Conditions of Møre & romsdal County .....	8
3.1 Temperature measurements within or near Møre & Romsdal County.....	8
3.2 Key factors controlling the subsurface temperature in the study are .....	12
3.2.1 Insulating thermal effect of low-conductivity sediments .....	13
3.2.2 Groundwater flow.....	14
3.2.3 Palaeoclimatic influence .....	15
4. 3D THERMA MODELLING .....	17
4.1 Methodology.....	18
4.1.1 Thermal boundary conditions .....	19
4.1.2 The thermal modelling workflow .....	20
4.2 Input data and thermal properties.....	21
4.2.1 Structural data .....	21
4.2.2 Thermal properties.....	22
4.3 Results of the 3D thermal modelling.....	25
5. DISCUSSION .....	28
5.1 Constraints problems and limitations of the methodology.....	28
5.2 Implication of the results to deep geothermal potential .....	29
6. CONCLUSIONS .....	30



## 1. INTRODUCTION

As part of a collaborative research initiative between the Geological Survey of Norway (NGU) and Møre & Romsdal County, a comprehensive assessment of the region's deep geothermal energy potential has been conducted. This evaluation is based on an analysis of available geological and geophysical datasets, including temperature measurements, subsurface structural interpretations, and existing lithosphere-scale 3D thermal models (Maystrenko & Gernigon, 2018; Maystrenko, 2019).

The study integrates multiple constraints, such as borehole thermal logs, laboratory-measured rock properties, heat flow density estimates, and regional tectonic features, to construct a temperature distribution model at significant depths within the study area. By integrating these diverse datasets, the research provides a better understanding of subsurface thermal conditions, helping to identify zones with favorable geothermal characteristics.

Beyond advancing scientific knowledge of Norway's deep geothermal resources, this work contributes to broader national and regional energy strategies. It supports the transition toward sustainable energy solutions by assessing the feasibility of geothermal systems as a realistic alternative to fossil fuels, thereby aiding in the reduction of greenhouse gas emissions and enhancing energy supply.

## 2. LARGE-SCALE GEOTHERMAL OVERVIEW

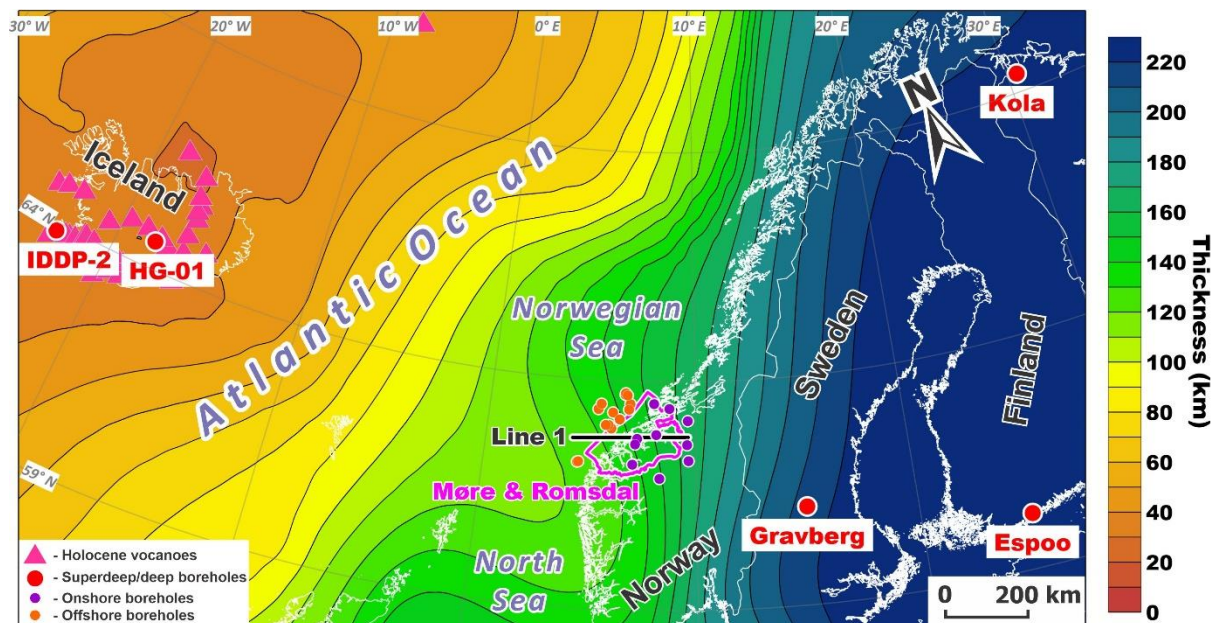


**Figure 1:** Map showing lithospheric thickness, derived from Steinberger and Becker (2018), together with the locations of deep and superdeep boreholes in Fennoscandia and Iceland. The boundaries of Møre & Romsdal County are highlighted in magenta. Both onshore boreholes and offshore hydrocarbon wells near the county are displayed. The position of temperature profile Line 1 is also indicated. The Holocene volcanoes distribution according to the data from Global Volcanism Program (2024).

The thickness of the lithosphere is a key controlling factor for deep temperature patterns in the Earth's crust and upper mantle. The lithosphere, Earth's solid outermost layer, acts as an insulating layer over the hotter, convecting asthenosphere. Its base is defined by the 1300–1333°C isotherm

(Turcotte & Schubert, 2002), marking the transition from solid rock above to molten material below. A thicker lithosphere restricts heat flow, leading to a colder subsurface. On the other hand, a thinner lithosphere allows faster heat escape, resulting in higher crustal temperatures. Consequently, a thicker lithosphere correlates with colder shallow crust (accessible via deep boreholes), while a thinner lithosphere leads to higher crustal temperatures. This regularity explains regional variations in heat flow, magma generation, and tectonic activity/stability. Although lithospheric thickness is the primary factor, other factors can modify deep thermal patterns.

The major three additional factors affecting the thermal regime of the subsurface are related to (1) crustal radiogenic heat production due to the internal decay of radioactive elements (e.g., uranium, thorium and potassium); (2) fluid circulation, represented by groundwater flow within the upper crust, which redistributes heat through advection, locally changing subsurface thermal patterns and (3) blanketing thermal effect of low-thermal conductive sediments, which slow down heat transfer from deeper levels toward the surface, effectively storing heat below the sediments.

Møre & Romsdal County occupies a place, located at the dynamic transition between two different lithospheric domains (Fig. 1). To the east, it borders the ancient and stable Fennoscandian Shield, a crystalline bedrock formation that extends across Russia, Finland, Sweden and Norway. Beneath this shield, the lithosphere reaches remarkable thicknesses of over 200 km, reflecting its long-term tectonic stability. In contrast, to the west, the county faces the North Atlantic Ocean, where the lithosphere thins dramatically to less than 10 km at the Mid-Oceanic Ridge. Therefore, this geological setting makes Møre & Romsdal a region of geothermal complicity since it is situated within a transition zone from the thick, rigid and cold continental lithosphere of Fennoscandia towards the much thinner, younger and warmer oceanic lithosphere.

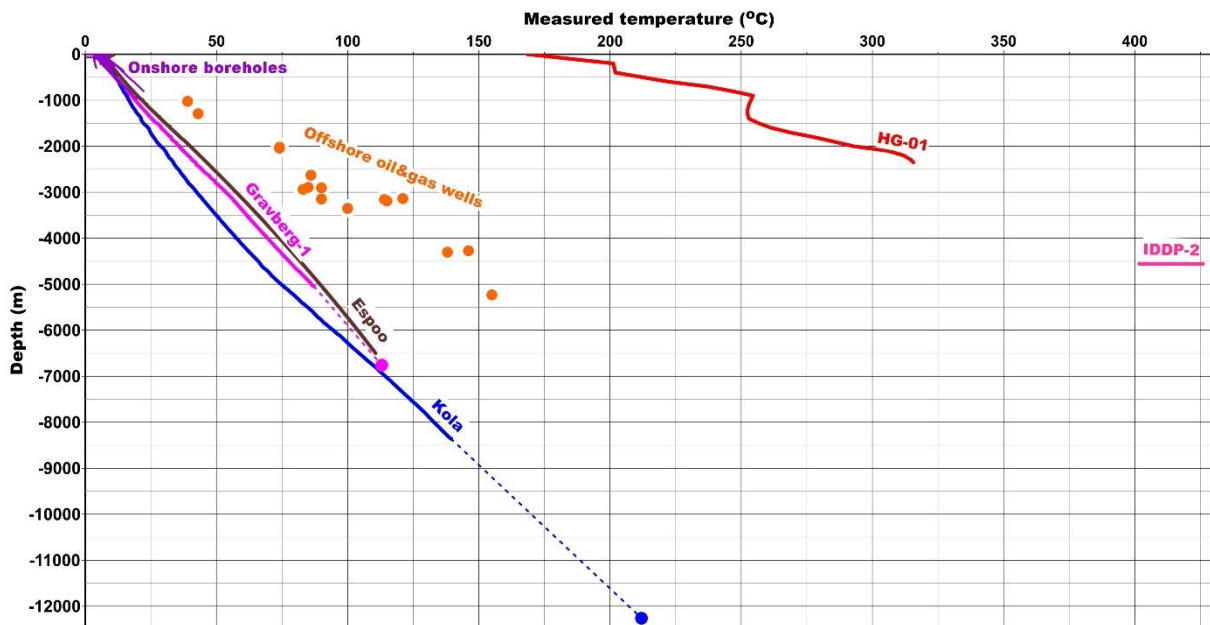


**Figure 2:** Plot showing the measured temperatures from superdeep boreholes in Sweden, Finland, and Russia (Popov et al., 1999; Popov, 1999; Balling, 2024; Heikkinen et al., 2021; Kukkonen & Pentti, 2021), compared to temperature data from Iceland (Seifu, 2004; Hokstad et al., 2017; Friðleifsson et al., 2020). Additionally, temperature logs from selected onshore boreholes (NGU and Asplan Viak measurements) are displayed together with bottom hole and drill stem test temperatures from the selected hydrocarbon wells onshore (NOD, 2024). The depth of onshore, both deep and superdeep, boreholes is shown relative to the Earth's surface, while the depth of offshore wells is referenced to sea level.

It is important to note that the precise thickness of the lithosphere beneath the study area remains uncertain, and the map in Figure 1 should be considered as a preliminary approximation rather than a detailed representation. Further research in this region could provide valuable insights into

lithosphere-asthenosphere interactions, whereas at present, it is essential to know that Møre & Romsdal represents not only a transition from thinner to thicker lithosphere but also a shift from the mainland, where crystalline rocks are exposed at the surface, to the deep sedimentary basins of the Mid-Norwegian continental margin.

The specific location of Møre & Romsdal is evident in the temperature variations measured in deep boreholes across the region. Relatively low temperatures have been recorded in superdeep boreholes in Sweden, Finland, and Russia, while significantly higher temperatures are measured in deep boreholes in Iceland (Fig. 2). This contrast is due to Iceland's position on the Mid-Atlantic Ridge, the boundary between lithospheric plates, where magma lies close to the surface, causing a significant temperature increase in the uppermost crust. The presence of active volcanoes further demonstrates that hot magmatic rock can even reach the surface.

Temperature measurements from onshore boreholes in Møre & Romsdal, which are less than 1 km deep, already exceed those from superdeep boreholes like Gravberg-1 in Sweden, Espoo in Finland, and Kola in Russia (Fig. 2). Furthermore, bottom-hole and drill stem test temperatures from selected onshore hydrocarbon wells are higher than those from central and eastern Fennoscandia's superdeep boreholes. Nevertheless, these temperatures remain much lower than those measured in Iceland.

Despite these higher temperatures, the offshore wells remain significantly lower than those observed in Iceland, where thin lithosphere and magmatic activity are responsible for one of the highest geothermal gradients globally. This comparison reveals the regional variability in subsurface thermal regimes, influenced by variations in lithosphere thickness.

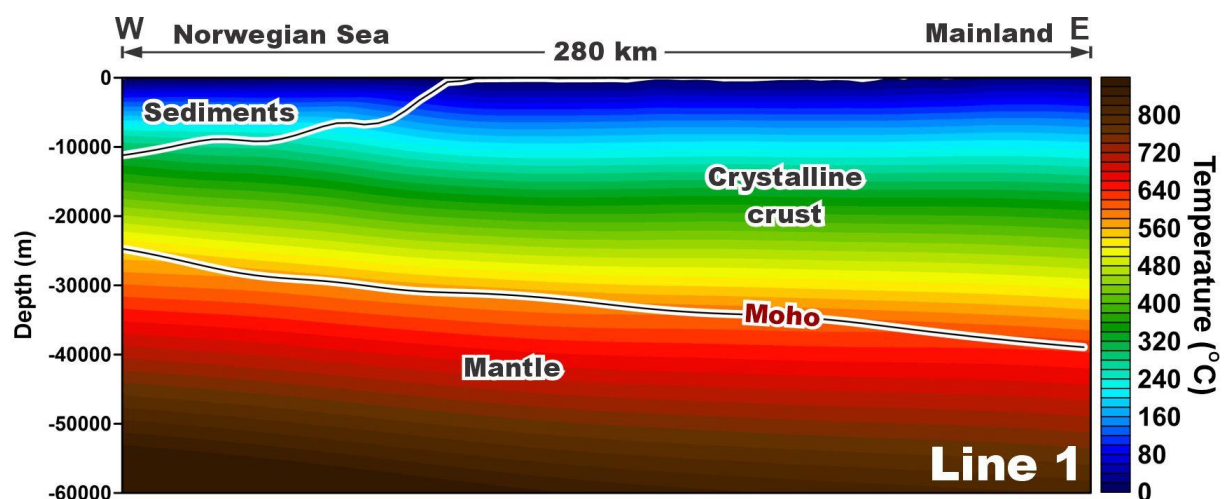


**Figure 3:** Profile showing the modelled subsurface temperatures along the selected 2D vertical cross-section through the 3D thermal model of the Mid-Norwegian continental margin (Maystrenko & Gernigon, 2018; see Figs. 1 and 4 for slice location). Vertical exaggeration is 2 times.

Therefore, the temperature increases from the near-coastal zones of the Møre & Romsdal mainland toward offshore areas according to the measured temperatures in the onshore boreholes and offshore oil&gas wells (Fig. 2). This is consistent with the results of regional-scale 3D thermal modelling (Maystrenko & Gernigon, 2018), as illustrated in Figure 3. This trend suggests a progressive increase in subsurface temperatures farther from the coast. The modelling results provide support for this thermal pattern in the lower crust and upper mantle, following the observed spatial temperature distribution within the upper crust.

### 3. SUBSURFACE THERMAL CONDITIONS OF MØRE & ROMSDAL COUNTY

#### 3.1 Temperature measurements within and near Møre & Romsdal County

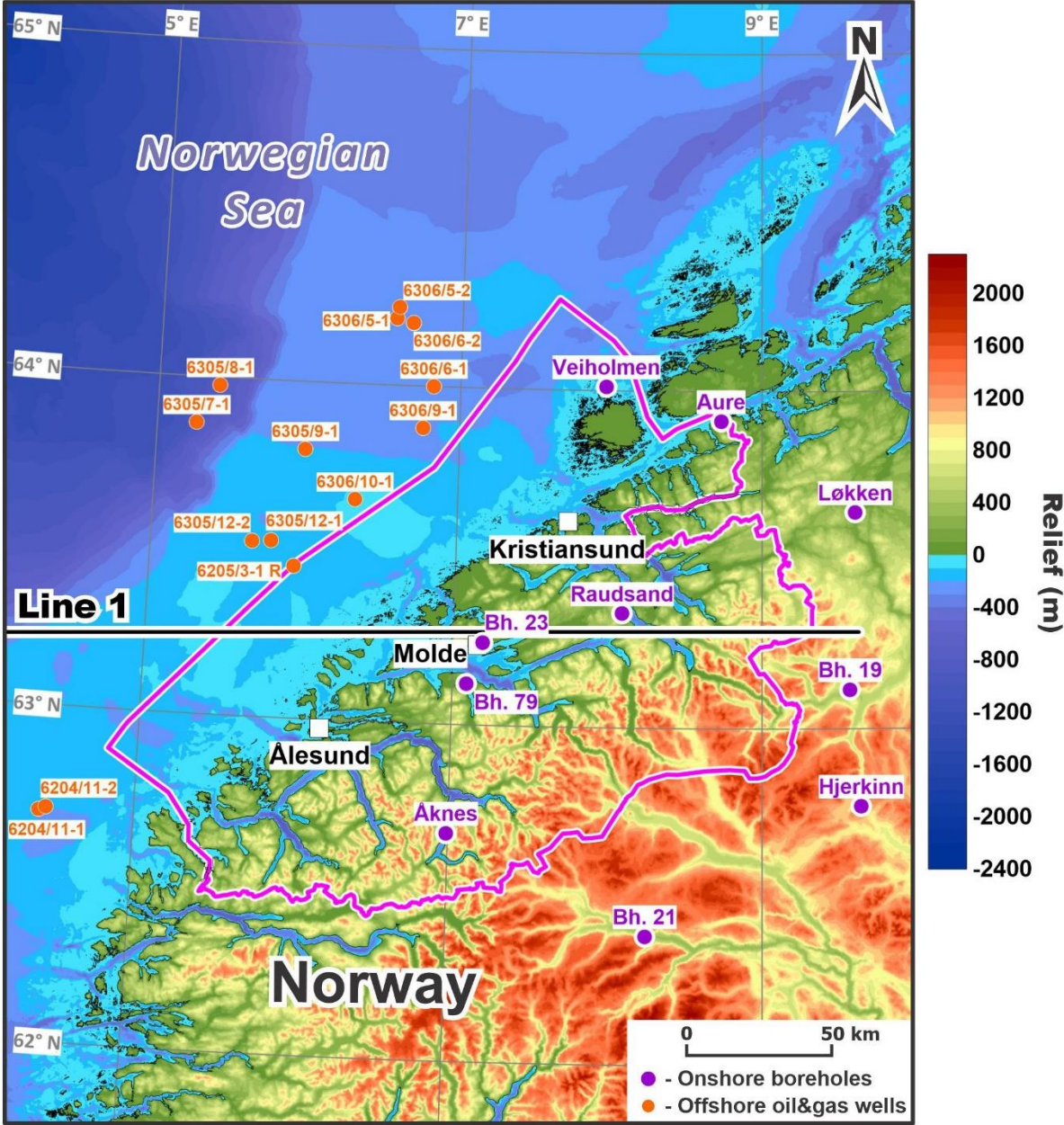


**Figure 4:** Overview map of the Møre & Romsdal region, showing the locations of available boreholes with temperature logs on the mainland, as well as offshore bottom-hole temperatures (BHT) and drill-stem test (DST) temperatures. The relief (topography and bathymetry) data were provided by the Norwegian Mapping Authority (Kartverket).

As already mentioned earlier, Møre & Romsdal County lies at the transition from thicker to thinner lithosphere at a large scale, extending from exposed crystalline bedrock on land to the deep offshore sedimentary basins at the Mid-Norwegian continental margin. These features are evident in the temperature data collected from the boreholes drilled in the region.

The map in Figure 4 shows the locations of selected onshore boreholes deeper than 200 m, together with nearby offshore hydrocarbon wells. The available onshore dataset includes temperature measurements from twelve boreholes within Møre & Romsdal County and four additional boreholes in close proximity to the county. However, eight of these boreholes are clustered in two distinct areas: four in the Åknes area and four in the Raudsand area, representing two sites rather than eight separate locations. Temperature well-logging in the Åknes, Aure, Hjerkin, Løkken, Raudsand and Veiholmen boreholes was conducted by NGU. Additionally, boreholes 19, 21, 23, and 79 are shallow geothermal wells, with temperature measurements provided by Asplan Viak. While the precision and accuracy of these measurements are lower than those from NGU, they help to fill data gaps between the more detailed NGU data.

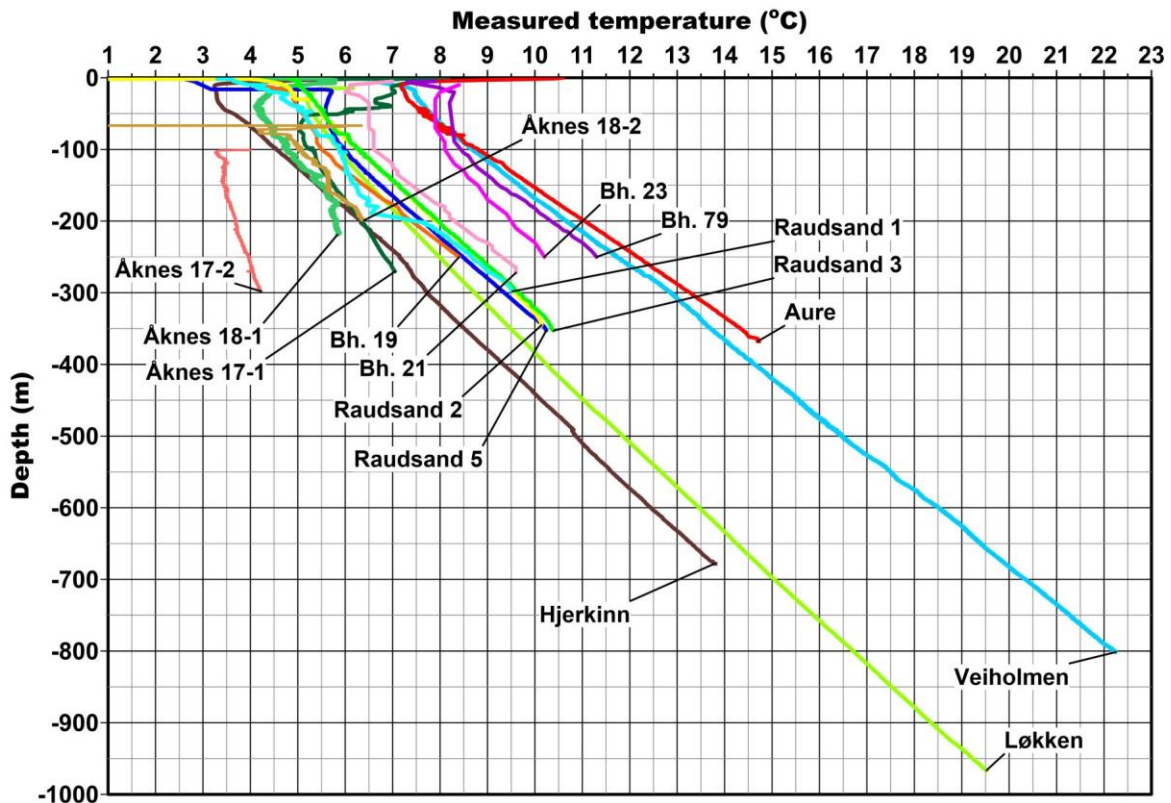


**Figure 5:** Plot showing the measured temperatures in the selected boreholes within the Møre & Romsdal County and the adjacent areas on the mainland. NGU data combined with Asplan Viak data for boreholes 19, 21, 23, and 79.

A detailed description of the temperature logging for the NGU boreholes is available in the following reports and manuscripts: the Åknes boreholes are described in Elvebakk and Pless (2018); the Aure (Kjørsvik), Hjerkin, and Løkken boreholes are covered in Balling and Breiner (2005); the Raudsand boreholes are documented in Elvebakk and Lutro (2017); and the Veiholmen borehole is detailed in Elvebakk (2019) and Maystrenko et al, (2021). The Åknes boreholes were drilled to investigate the possibility of draining the landslide-prone mountain area. The purpose of drilling the Aure borehole is not known. The Hjerkin and Løkken boreholes were drilled within the respective mines for mineral prospecting. The Raudsand boreholes were drilled to assess large rock storage facilities for inorganic hazardous waste. The Veiholmen borehole was drilled by NGU as part of the oil and gas industry-funded project COOP3, aiming to study the composition of basement rocks and the thermal state of the area near the Frøya High.

**Table 1:** List of the selected onshore boreholes with the measured temperature.

Borehole name	WE, UTM32N	NS, UTM32N	Bottom hole temperature, °C	Depth below Earth's surface, m	Altitude. m
<b>NGU measurements</b>					
Åknes 17-1	395716	6895672	7,05	270,34	506,8
Åknes 17-2	395369	6895890	4,228	298,03	733,7
Åknes 18-1	395318	6895693	5,84	218,97	592,9
Åknes 18-2	395448	6895529	6,396	199,04	482
Aure	486454	7031460	14,7	367,74	5
Loekken	530797	7001453	19,52	966,49	310
Hjerkinn	532846	6904427	13,78	678,18	960
Raudsand 1	454333	6968628	9,52	298,11	245
Raudsand 2	453606	6968294	10,14	345,26	315
Raudsand 3	453788	6968322	10,39	352,9	298
Raudsand 5	453710	6968058	10,24	352,63	349
Veiholmen	448535	7043010	19,54	801,3	3
<b>Asplan Viak measurements</b>					
Bh. 19	529138	6942956	8,4	250	-
Bh. 21	461179	6861330	9,6	272	-
Bh. 23	407651	6958395	10,2	250	-
Bh. 79	402081	6944862	11,3	250	-

The detailed descriptions of the Asplan Viak boreholes are not publicly accessible. All these boreholes were drilled for shallow geothermal heat extraction. Specifically, Borehole 19 supplies heat to Midtbygda School, Borehole 21 serves Skjåk School, Borehole 23 supports Romsdal High School in Molde, and Borehole 79 provides heating for Vestnes Nursing Home.

The measured temperatures from the onshore boreholes are presented in Figure 5, illustrating the thermal state of the subsurface at depths ranging from nearly 200 m to almost 1 km. Unfortunately, no deeper onshore boreholes exist in Møre & Romsdal. As shown in Figure 5, the thermal pattern indicates a gradual increase in temperature from inland areas toward the near-coastal regions (cf. Figs. 4 and 5). This trend is particularly evident in the three deep boreholes, the Løkken, Hjerkinn, and Veiholmen boreholes, where temperatures rise distinctly from the Hjerkinn site through the Løkken area to the Veiholmen borehole. The nearly 960 m altitude of the Hjerkinn borehole location likely contributes to its relatively low temperature, whereas the Løkken borehole is situated at a much lower elevation (Table 1). The shallower boreholes also support this temperature trend, confirming that this thermal pattern is not coincidental. However, the temperature measurements in the Åknes boreholes are not fully representative of their respective depths. The thermal regime in these boreholes is influenced not only by vertical heat transfer but also by horizontal heat

conduction due to their proximity to steep mountain slopes. Additionally, the Åknes boreholes are significantly affected by groundwater flow, which will be discussed in more detail later.

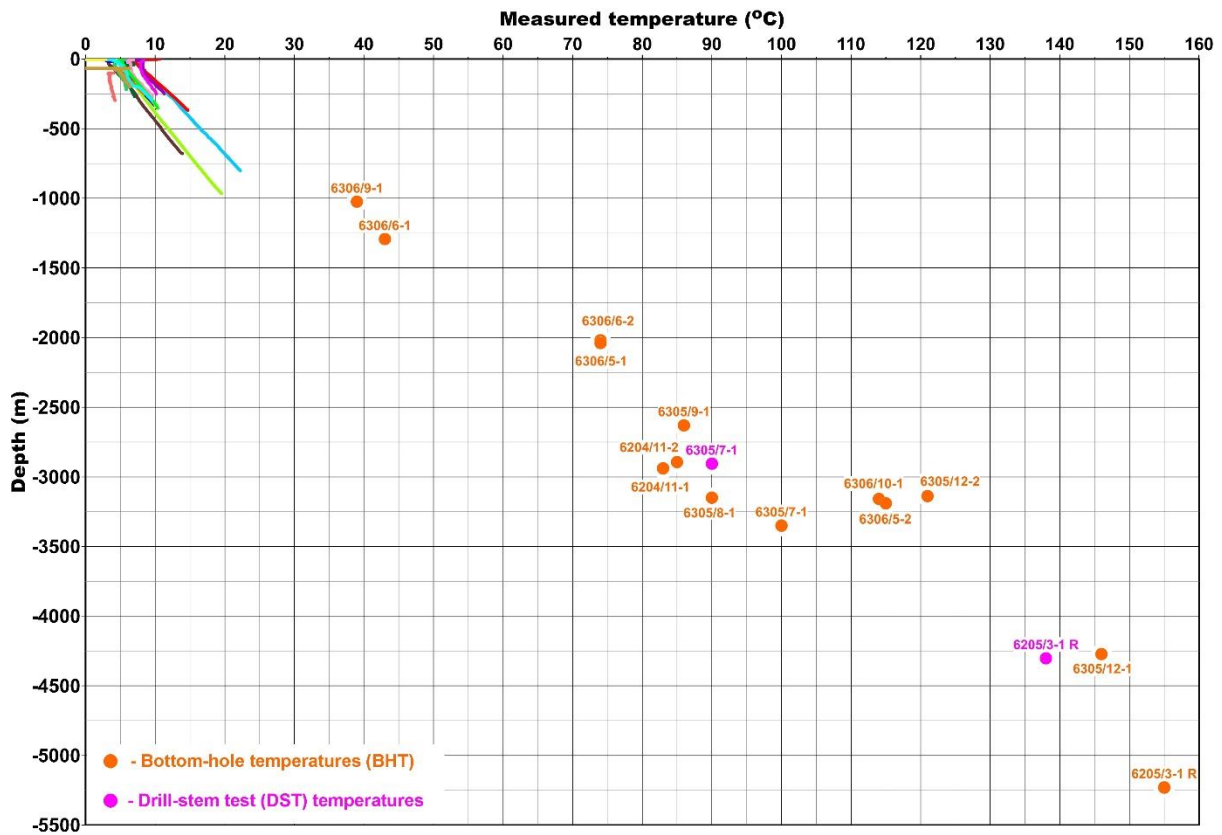


**Figure 6:** Plot showing the measured temperatures in the selected onshore boreholes within the Møre & Romsdal County and the adjacent areas (NGU data combined with Asplan Viak data) and bottom hole and drill stem test temperatures from the selected hydrocarbon wells onshore (NOD, 2024).

Therefore, a clear trend of increasing temperatures toward the coast is evident. This factor must be considered in future deep geothermal drilling projects. To better understand this pattern, temperature data from nearby offshore hydrocarbon wells have been taken into account as well. The available measurements from the offshore wells are plotted in Figure 6 together with the onshore borehole data. Notably, temperatures recorded offshore are even higher than those observed in the near-coastal onshore boreholes. This contrast would be even more pronounced if offshore temperatures were referred to the seafloor rather than sea level, as illustrated in Figure 6. Among the selected offshore wells, the more distant ones (6305/7-1 and 6305/8-1) show lower temperatures at comparable depths than those closer to the coast (e.g. 6305/12-2 and 6306/10-1) (cf. Figs. 4 and 6). This discrepancy can be at least partly attributed to the significant difference in water depth: wells 6305/7-1 and 6305/8-1 are drilled at water depths exceeding 800 m, whereas 6305/12-2 and 6306/10-1 are located in shallower waters, less than 150 m (Table 2). This over 650 m difference in vertical depth further supports the observed trend of increasing temperatures at equivalent depths when moving from the near coastal areas toward the open ocean.

It is important to note that bottom-hole temperatures were recorded near the base of the wells either during or shortly after drilling. Therefore, these measurements are often unreliable due to thermal disturbances caused by drilling fluid circulation (which cools the bottom) and frictional heat generated during drilling. In contrast, drill-stem test temperatures reflect equilibrium conditions between formation fluids and surrounding sedimentary rocks, offering more accurate thermal data. Unfortunately, only two drill-stem test temperatures are available for the study area (Fig. 6).

Nevertheless, deviations in bottom-hole temperatures could not destroy the observed thermal trend due to the significant temperature difference between onshore and offshore measurements.

**Table 2:** List of the selected offshore hydrocarbon wells (NOD, 2024).

Well name	WE, UTM32N	NS, UTM32N	Bottom hole temperature, °C	Depth below sea level, m	Sea water depth. m
6205/3-1 R	344993	6983968	155	5230	159
6305/7-1	313104	7031511	100	3350,9	857
6305/8-1	320901	7043695	90	3149,8	837
6305/9-1	349013	7022561	86	2630	187
6306/10-1	365423	7005917	114	3158	83
6306/5-1	379385	7065777	74	2019	227,5
6306/6-1	391521	7043191	43	1293	284
6306/9-1	387942	7029466	39	1025	228
6305/12-1	337587	6992299	146	4273	176,5
6305/12-2	331419	6992168	121	3138	146
6306/5-2	380274	7069474	115	3190,5	226
6306/6-2	384838	7064163	74	2039,8	224
6204/11-1	260665	6903634	83	2939,6	199
6204/11-2	263045	6904506	85	2894	197
Well name	WE, UTM32N	NS, UTM32N	Drill-stem test temperature, °C	Depth below sea level, m	Sea water depth. m
6205/3-1 R	344992,78	6983968,16	138	4302,7	159
6305/7-1	313103,74	7031511,44	90	2906	857

The highest temperature of 155°C was recorded in well 6205/3-1R at a depth of 5230 meters (Fig. 6; Table 2). This temperature meets the threshold for direct electric power generation. While the measurement represents bottom hole temperature, which may show minor deviations from the given temperature, a temperature correction will most likely increase this already high value.

### 3.2 Key factors controlling the subsurface temperature in the study area

Certainly, the thinning of the lithosphere toward the ocean plays a significant role. However, this factor alone cannot explain the pronounced temperature variations observed across Møre & Romsdal County and adjacent regions (Fig. 6). At least three other key factors contribute to these variations, including the insulating thermal effect of low-conductivity sediments, groundwater flow dynamics and palaeoclimatic influence.

### 3.2.1 Insulating thermal effect of low-conductivity sediments

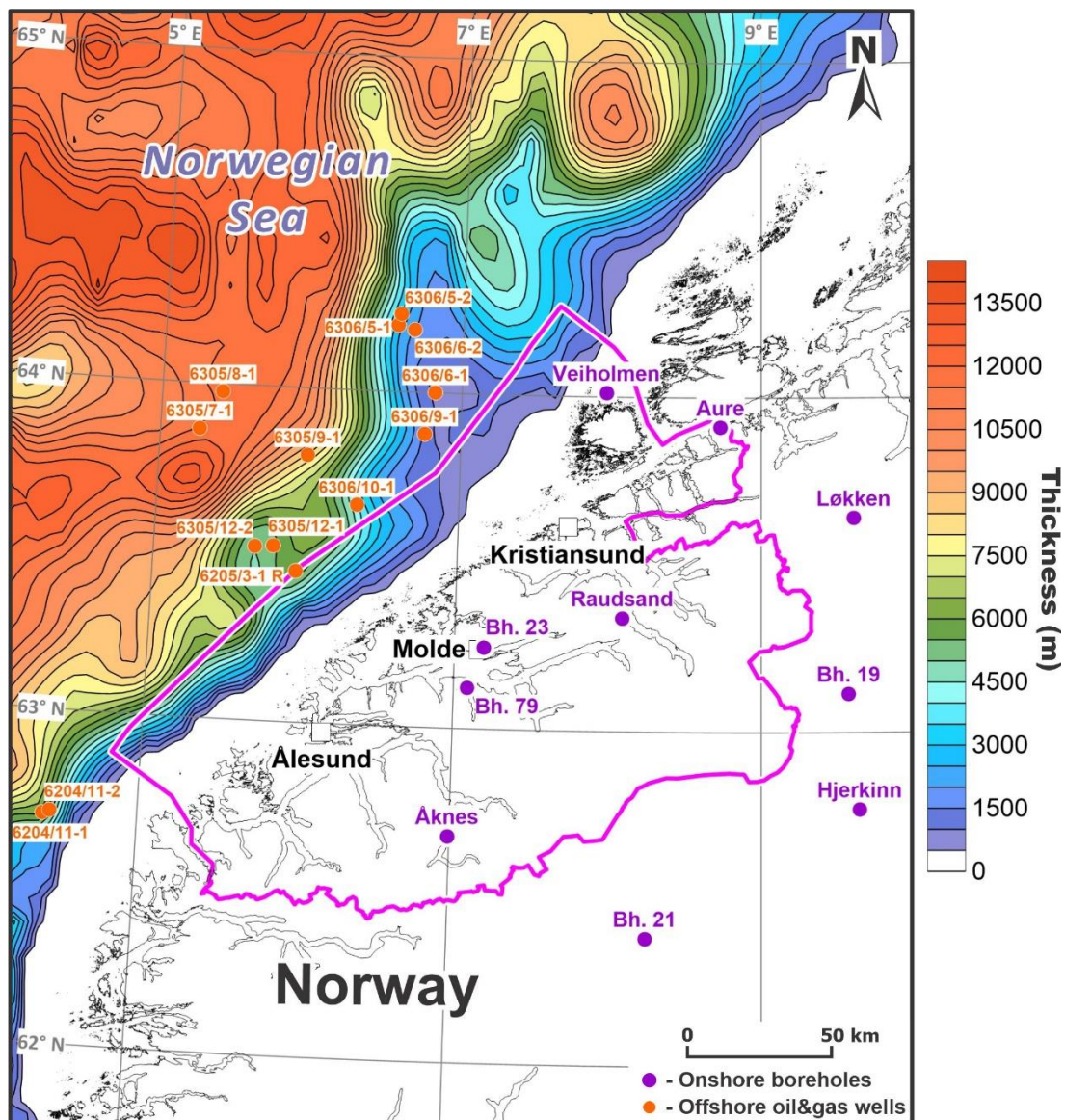


**Figure 7:** Map showing the total thickness of sedimentary rocks in the Norwegian Sea near Møre & Romsdal County (based on Maystrenko et al., 2018; layers 2, 3, 4, 6, 7, 8 in Table 3).

A distinct contrast exists between the mainland and offshore regions of Møre & Romsdal in terms of sedimentary cover. The mainland is predominantly characterized by exposed crystalline rocks, without thick sedimentary sequences above. Only thin Quaternary deposits are occasionally present onshore. In contrast, the offshore Mid-Norwegian Continental Margin hosts extensive Paleozoic, Mesozoic, and Cenozoic sedimentary successions within the adjacent Møre Basin and Trøndelag Platform, where total thickness of the sedimentary cover exceeds 10 km (Fig. 7). Near the coast, thickness of sediments increases rapidly from zero to over 6 km within relatively short distances, particularly offshore Molde and Ålesund (Fig. 7).

Thermal conductivity differences between crystalline and sedimentary rocks play a key role in heat distribution. Crystalline rocks exhibit higher thermal conductivity, promoting efficient heat escape (the so-called chimney effect). In contrast, thick, low-conductivity sedimentary layers, particularly young, porous sediments, act as thermal insulators, storing heat beneath them (the so-called blanketing effect). The combined influence of these effects leads to elevated subsurface temperatures offshore, where thick sediments dominate, while onshore areas experience greater

heat escape due to the very thin sedimentary cover or its absence. In particular, the uppermost Cenozoic sedimentary successions on the Mid-Norwegian margin have the lowest thermal conductivities, contributing to higher measured temperatures within the sedimentary cover in the offshore wells compared to the onshore ones.

### 3.2.2 Groundwater flow

Another important factor, influencing subsurface thermal conditions is related to groundwater flow. While this phenomenon may not have a broad regional impact, its local thermal effect can be significant. This is particularly evident in areas with intense groundwater flow, where the circulation of water can significantly affect temperature distributions within the subsurface. A clear example of this effect is illustrated by Figure 8, which shows temperature logs from the selected onshore boreholes with strong groundwater flow. These logs demonstrate notable deviations from expected geothermal gradients, highlighting how advective heat transfer, driven by groundwater flow, can change the thermal profile of the subsurface. Active groundwater flow within these boreholes is responsible for the relatively high amplitude peaks in the temperature curves (Fig. 8). Even vertical water flow, both upward and downward, has been detected in the Åknes boreholes, reaching rates of approximately 2400 l/h (Elvebakk & Pless, 2018). Similarly, in the Raudsand borehole 1, strong downward water flow was audibly observed (Rønning et al., 2017) and temperature irregularities (Fig. 8) most likely indicate water intrusions through fracture zones.

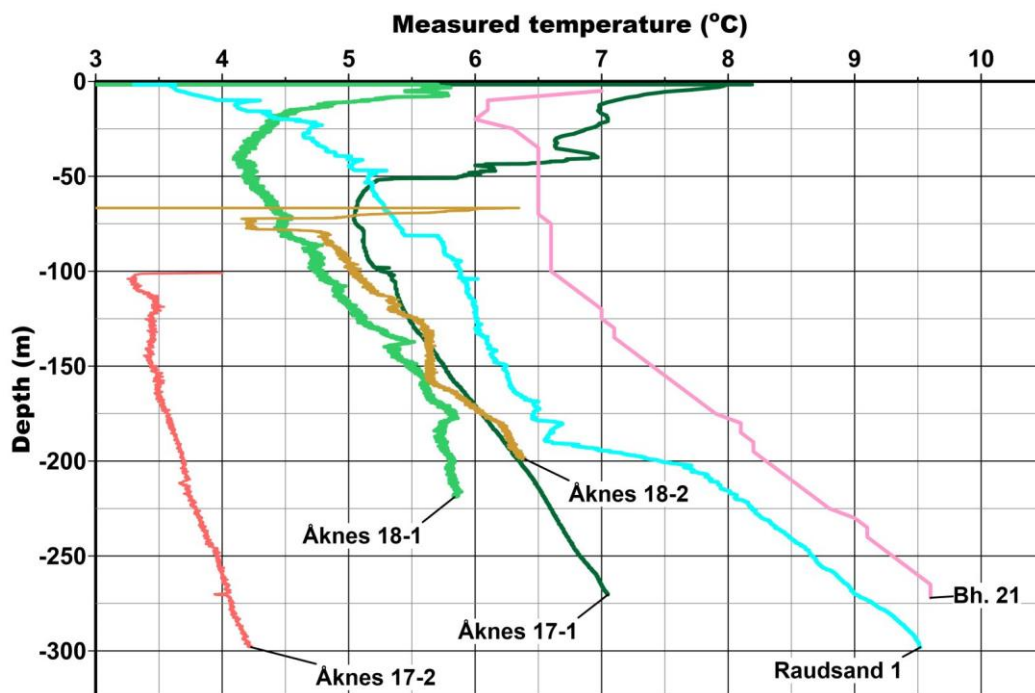


**Figure 8:** Plot showing the temperature logs, influenced by groundwater flow (NGU data combined with Asplan Viak data).

Such strong variations point to the importance of considering hydrological conditions when assessing subsurface thermal regimes, even if their influence is not uniformly distributed across the Møre & Romsdal region. In general, there are hundreds of groundwater boreholes in Møre & Romsdal that indicate groundwater flow within the first hundred meters of the subsurface (GRANADA - National Groundwater Database, 2025). However, evidence of deep, strong groundwater flow is lacking, as the only deep Veiholmen borehole was drilled in the region. These local but potentially strong thermal perturbations point to a need for specific investigations during future geothermal studies, particularly in the areas where high-permeability fracture zones and

significant hydraulic/topographic gradients may enhance groundwater-driven heat redistribution within Møre & Romsdal County.

### 3.2.3 Palaeoclimatic influence

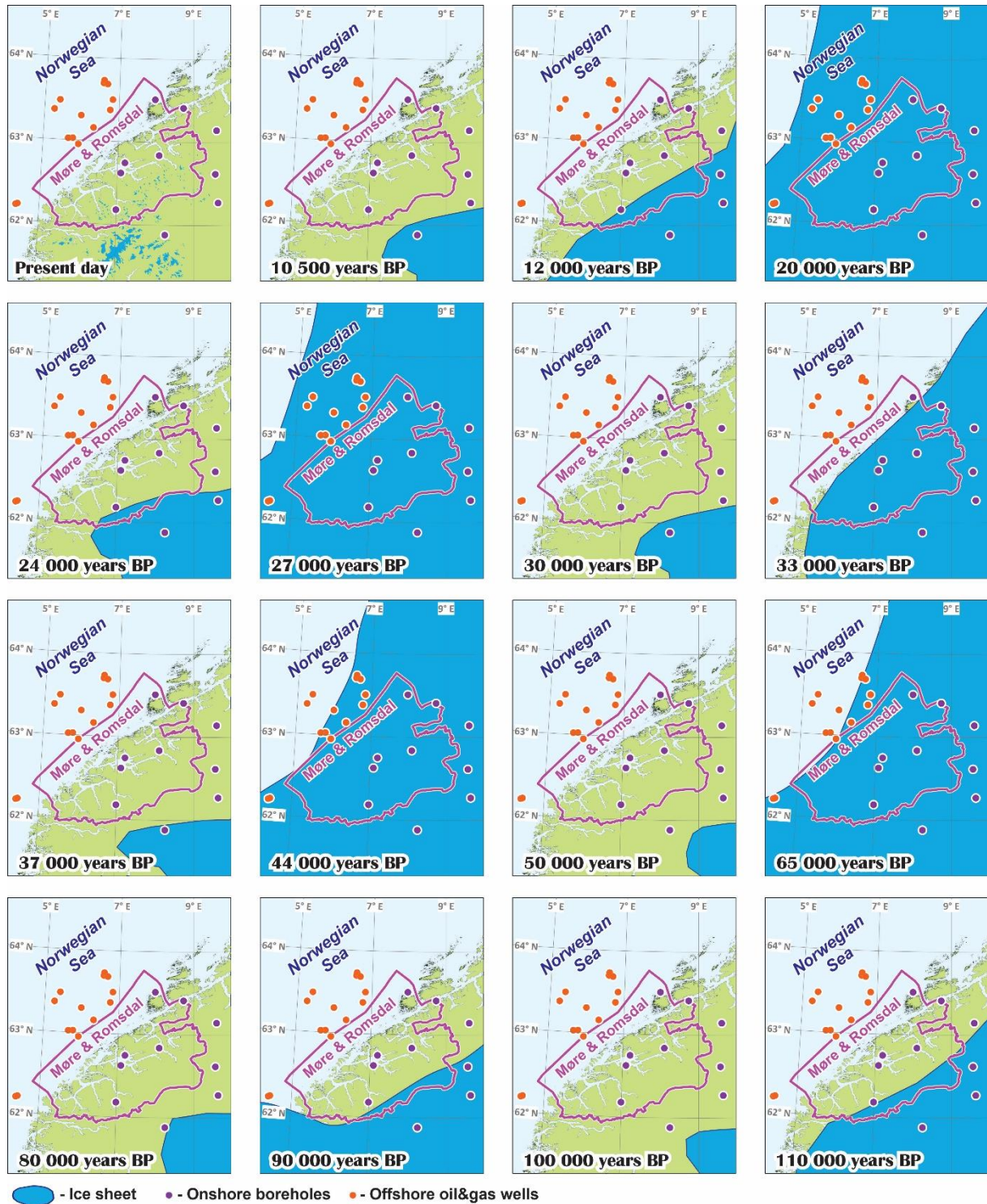


**Figure 9:** Maps showing dynamics of the ice cover during the Weichselian glaciation (after Olsen et al., 2013). Møre & Romsdal County is outlined in magenta, with selected onshore boreholes and offshore hydrocarbon wells displayed.

The next important factor is associated with the alternating sequence of cold and warm periods during the Quaternary. It is well known that Norway was entirely covered by an ice sheet during the last glacial period when the air temperature was much colder than today (e.g., Olsen et al., 2013). This cooling also penetrated the subsurface, leaving a persistent thermal signature, similar to how the ground remains cold long after winter.

The impact of the ice age was particularly intense in regions without the ice sheet, with its influence persisting at depths of up to 2 km. A critical factor is that the thick ice sheet (1–3 km in thickness) acted as a thermal insulator, shielding the ground from extremely cold open-air conditions during the last glaciations. In Møre & Romsdal, where onshore boreholes were frequently exposed to free-air conditions due to the partial absence of the ice cover (Fig. 9), subsurface cooling was more pronounced than in regions under continuous ice cover within the central Fennoscandia. As a result, temperature measurements from these onshore boreholes (Fig. 6) still reflect the ancient cooling events, displaying a disturbed thermal profile. To accurately predict deeper geothermal conditions, these palaeoclimate-related disturbances must be corrected. A slight temperature increase is expected at approximately 2 km depth, marking a transitional zone that separates the strongly disturbed upper thermal regime from the relatively undisturbed deeper levels.

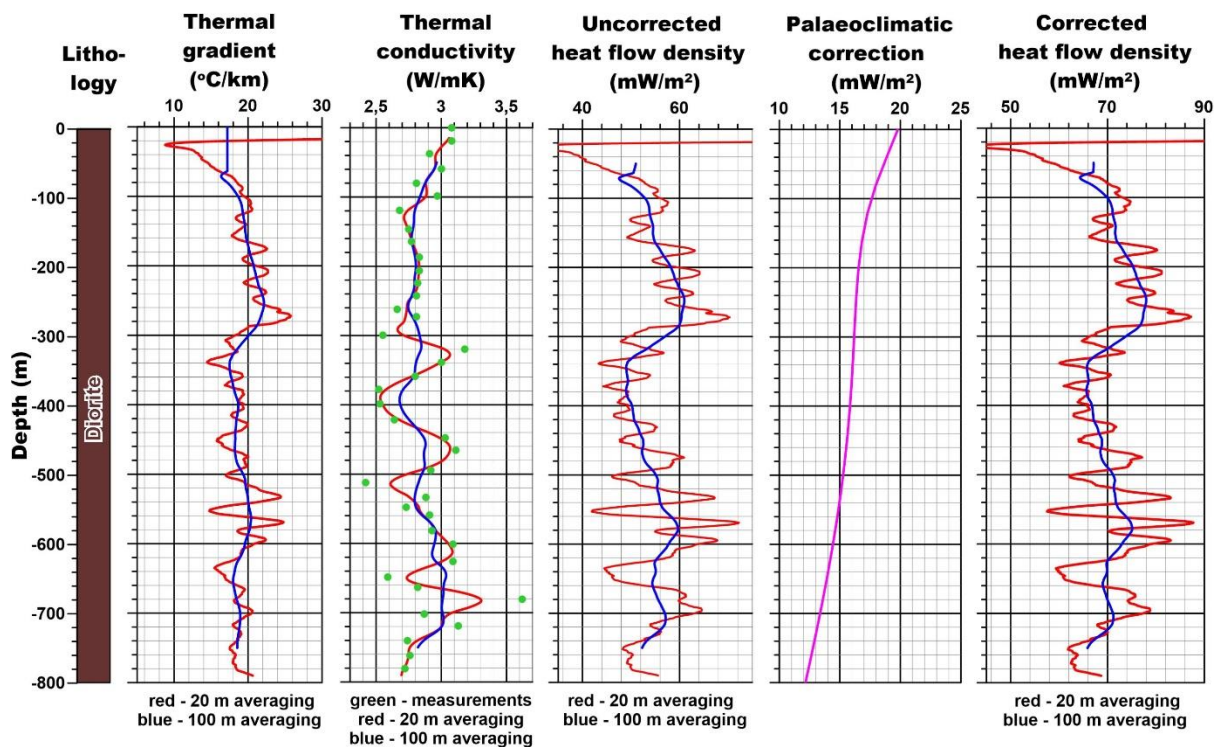


**Figure 10:** Plots showing lithology, thermal gradient, thermal conductivity, calculated uncorrected heat flow density, palaeoclimatic correction and calculated corrected heat flow density in the Veiholmen borehole (from Maystrenko et al. 2021).

The thermal impact of the last glacial periods is clearly demonstrated by palaeoclimatic corrections applied to calculated heat flow density for the Veiholmen borehole (Fig. 10). According to Maystrenko et al. (2021), this influence can be significant, reaching up to 20 mW/m<sup>2</sup>, in the case of the Veiholmen borehole. Although the palaeoclimatic signal diminishes with depth, its effects remain important and must be accounted for even at approximately 2 km depth. This persistent influence highlights the importance of correcting for past climate variations when interpreting subsurface thermal regimes, particularly in regions affected by Pleistocene glaciations, such as the Møre & Romsdal region.

#### 4. 3D THERMA MODELLING

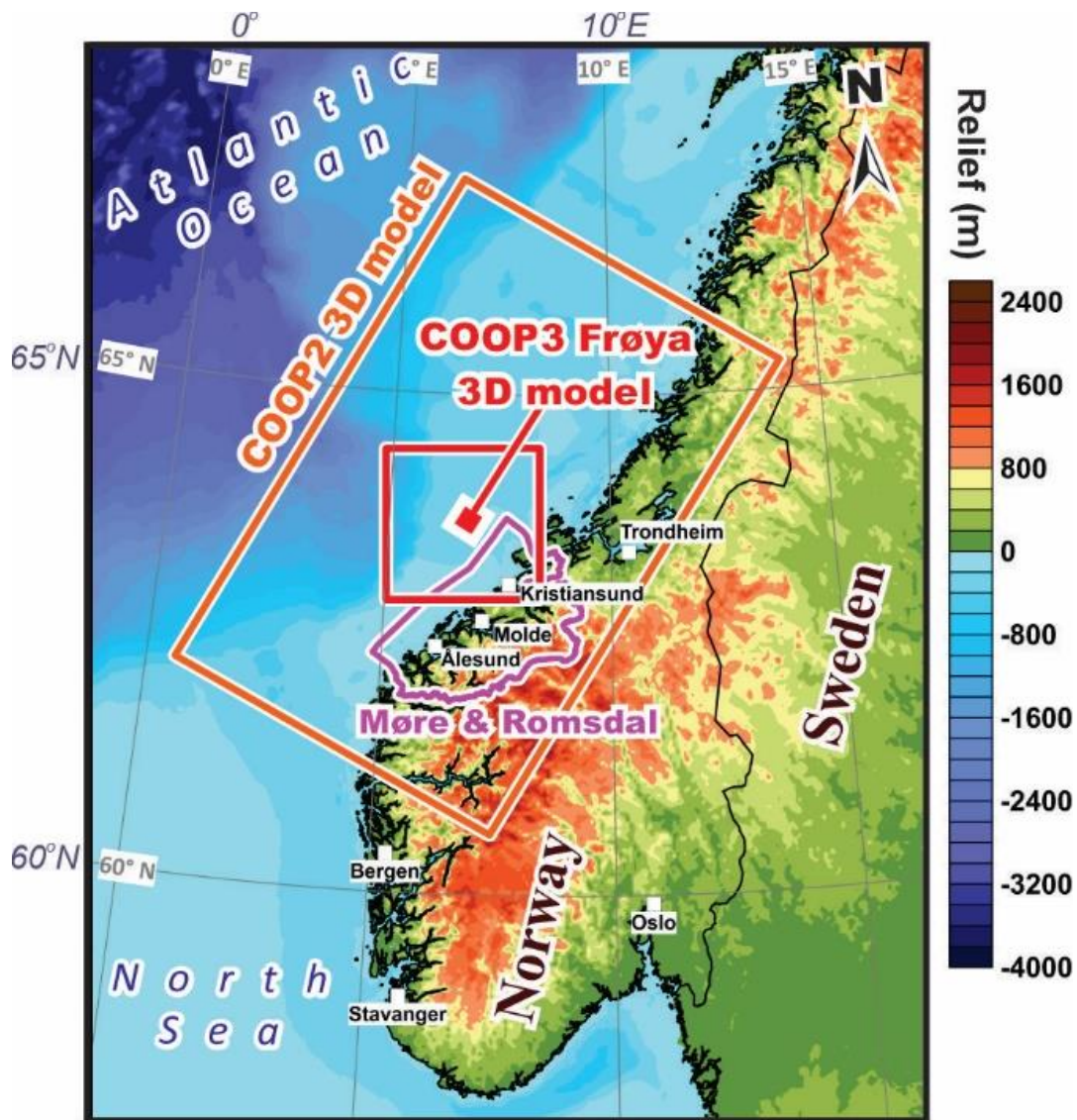


**Figure 11:** Overview map of western Scandinavia (relief from the Norwegian Mapping Authority) with the location of two 3D thermal models: (1) the COOP2 lithosphere-scale 3D thermal model of the Mid-Norwegian continental margin and adjacent mainland (Maystrenko & Gernigon, 2018; orange frame) and (2) the lithosphere-scale 3D thermal model of the Frøya area (Maystrenko, 2019; red frame).

The 3D temperature distribution across the Møre & Romsdal area was calculated by combining two existing lithosphere-scale thermal models (Figs. 11 and 12): (1) the regional 3D thermal model of the Mid-Norwegian continental margin, covering the Vøring and Møre basins and adjacent mainland (Fig. 12a; Maystrenko & Gernigon, 2018) and (2) a more detailed 3D thermal model of the Frøya High and its surrounding areas (Fig. 12b; Maystrenko, 2019). The second is a more detailed 3D thermal model focusing specifically on the Frøya High and its surrounding regions (Fig. 12b; Maystrenko, 2019). While the Frøya High model offers higher resolution in its coverage area, its spatial extent is limited compared to the broader Mid-Norwegian margin model, meaning it does not fully cover the entire Møre & Romsdal County (Fig. 11). To achieve a comprehensive thermal representation, the large-scale Mid-Norwegian margin model was refined by incorporating some structural details from the Frøya High model, along with additional constraints for the mainland.

However, due to time and data limitations, it still lacks the necessary resolution to fully represent all fine-scale subsurface structural variations across Møre & Romsdal County, particularly in complex geological zones where local heterogeneities can significantly influence temperature distributions.

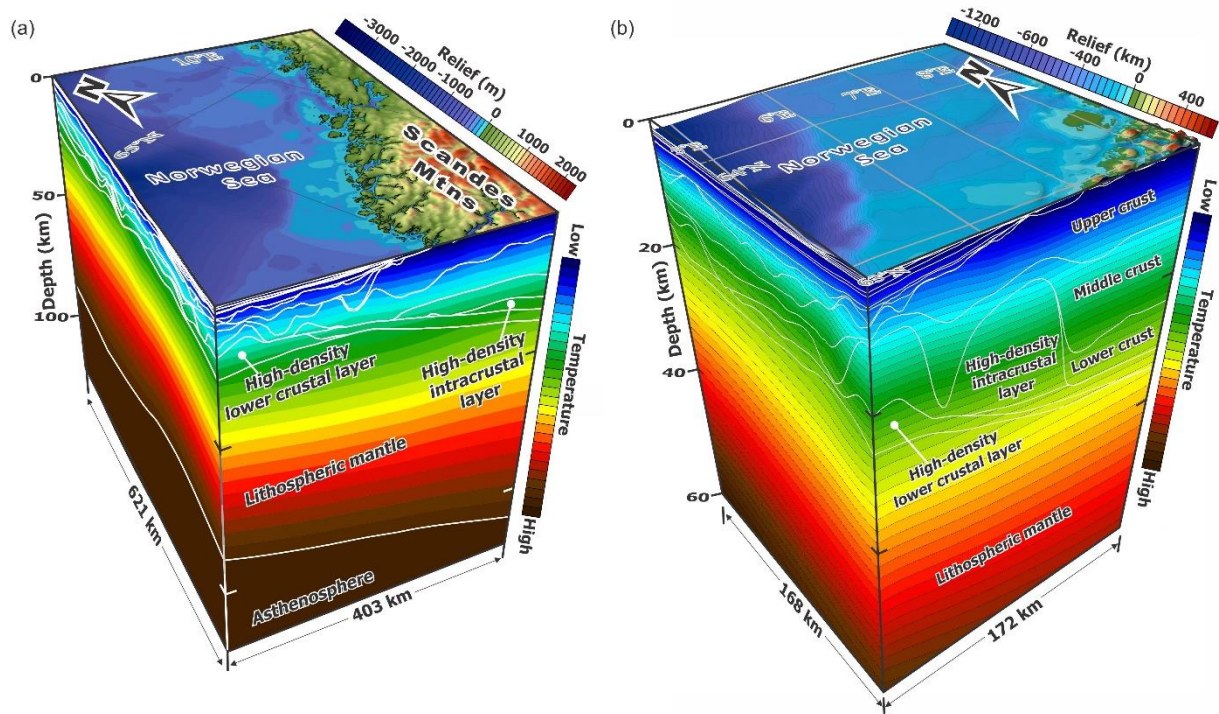


**Figure 12:** 3D temperature distributions within: (a) the lithosphere-scale 3D model of the Mid-Norwegian continental margin and adjacent areas of the Norwegian mainland (Maystrenko & Gernigon, 2018) and (b) the lithosphere-scale 3D model of the Frøya high area (Maystrenko, 2019).

#### 4.1 Methodology

The detailed descriptions of the methodology are available in Maystrenko & Gernigon (2018) and Maystrenko (2019). Only the key details are provided here.

The 3D temperature distribution across the structurally complex model of the Mid-Norwegian continental margin and adjacent mainland was computed using the commercial finite-element analysis software COMSOL Multiphysics. This software is widely used for simulating diverse physical processes. For the 3D thermal modelling, the Heat Transfer Module was utilized to simulate both steady-state and transient heat transfer in solid materials by thermal conduction, which is the dominant heat transfer mechanism at the regional scale within the subsurface of the study area. The calculations were based on the physical principles of conductive thermal fields, implemented through the numerical solution of the heat equation (1):

$$\rho C_p (\partial T / \partial t) = \nabla \cdot (k \nabla T) + Q \quad (1)$$

where  $\rho$  is density [ $\text{kg/m}^3$ ],  $C_p$  is specific heat capacity [ $\text{J/kg}\cdot\text{K}$ ],  $T$  is temperature [ $\text{K}$ ],  $k$  is thermal conductivity [ $\text{W/m}\cdot\text{K}$ ],  $\nabla T$  is the temperature gradient [ $\text{K/m}$ ],  $t$  is time [ $\text{s}$ ],  $Q$  is internal heat production (radioactive heat production) [ $\text{W/m}^3$ ],  $\partial T / \partial t$  represents the temporal temperature change, and  $\nabla \cdot (k \nabla T)$  accounts for spatial variations in temperature.

The solution of this equation depends critically on the thermal properties (specific heat capacity, thermal conductivity, and radiogenic heat production), density, and the imposed thermal boundary conditions (Fig. 13).

#### 4.1.1 Thermal boundary conditions

The thermal modelling was conducted in 3D, a suitable approach given the complex geometry of the Mid-Norwegian continental margin and adjacent areas. The lateral boundaries were defined as thermally insulated, preventing heat transfer by assuming a zero temperature gradient across them. For the upper thermal boundary condition, time-dependent temperatures at the seafloor and Earth's surface (Fig. 13) were applied. The base of the lithosphere (Fig. 13) served as the lower thermal boundary, corresponding to the conventional 1300 °C isotherm (Turcotte & Schubert 2002).

The present-day surface temperature of the Earth (Fig. 3a) is based on the 1961–1990 annual average air temperatures for the region, taken from the Norwegian Meteorological Institute (Tveito et al. 2000) and the National Atlas of Sweden (Raab & Vedin 1995). Seafloor temperatures were derived from published sea bottom temperature data in the Norwegian Sea (Ottersen 2009; Korablev et al. 2014) with values adjusted according to bathymetry. Additionally, seasonal average seafloor temperatures from the North Sea (1997–2002; ICES 2012) were used to validate temperatures in the northernmost part of the model area.

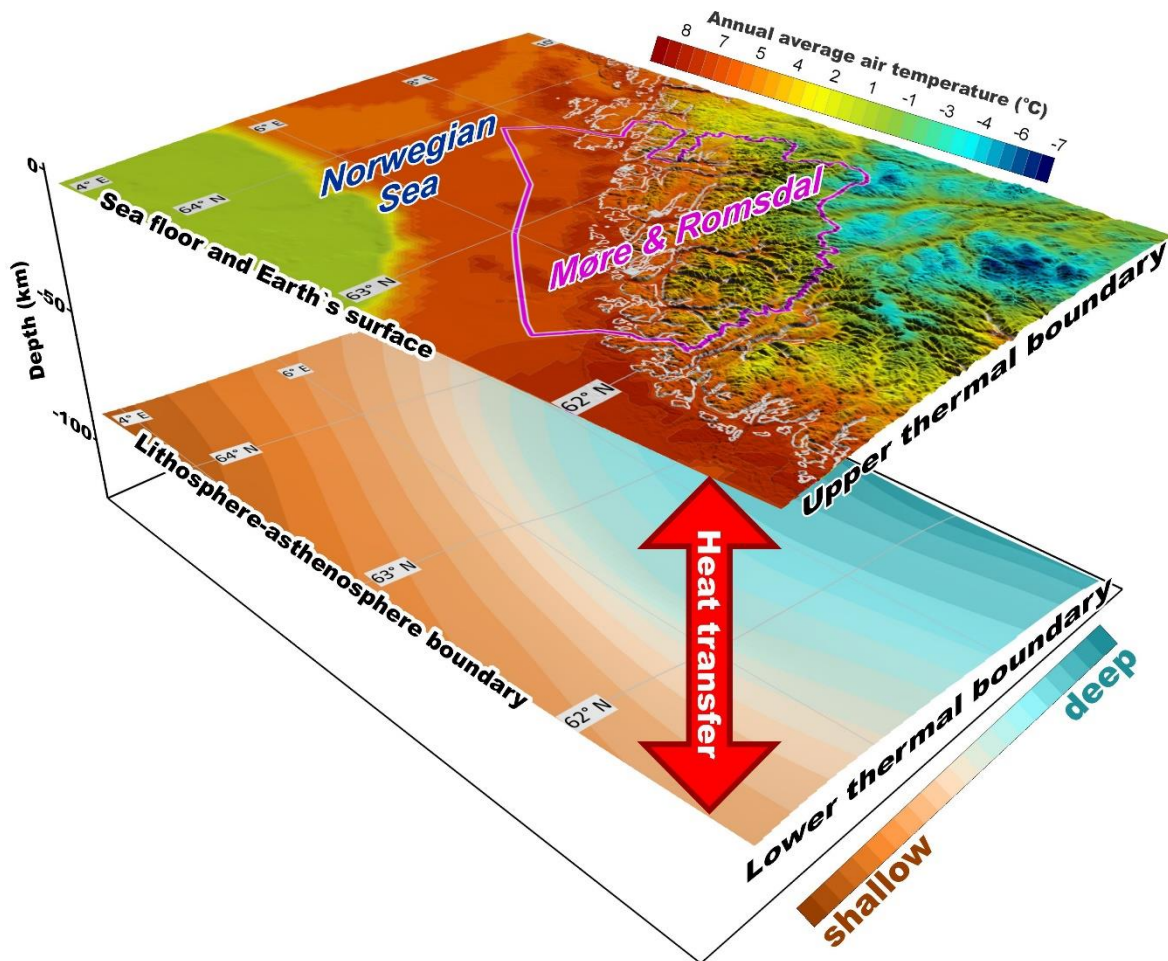


**Figure 13:** Schematic illustration displaying 3D conductive heat transfer calculation between thermal boundaries. The present-day upper thermal boundary is defined by annual average air temperatures (1961–1990) over Norway (Tveito et al., 2000) and sea-bottom temperatures derived from Ottersen (2009), ICES (2012), and Korablev et al. (2014). The lower thermal boundary corresponds to the 1300 °C isotherm at the lithosphere-asthenosphere boundary.

The 3D thermal modelling workflow also incorporates the detailed palaeoclimatic variations in surface temperature over the past 228,000 years before present. To reconstruct palaeoclimatic thermal conditions at the Earth's surface across Møre & Romsdal County, a model of spatio-temporal ice cover variations in Scandinavia during the Weichselian glacial period has been used, based on maps from Olsen et al. (2013). Figure 9 illustrates the ice cover distribution together with the position of Møre & Romsdal County, the selected onshore boreholes and the offshore hydrocarbon wells. According to Olsen et al. (2013) and Siegert et al. (2001), the study area was not continuously covered by a dynamic Weichselian ice sheet, which reached up to 3 km thickness during the Last Glacial Maximum. The same palaeoclimatic scenario was extended to the Saalian glacial and Eemian interglacial periods (220,000–118,000 years BP), as climatic conditions during these phases were broadly comparable to those of the Weichselian glacial and Holocene interglacial (Andersen & Borns 1994; Slagstad et al. 2009).

During glaciation, a subglacial temperature of  $-0.5\text{ }^{\circ}\text{C}$  was set at the Earth's surface beneath the ice cover, consistent with estimates for Antarctic ice sheets (Pattyn, 2010). This assumption is supported by the presence of subglacial lakes in Antarctica (Price et al., 2002) and drilling at Lake Vostok (Jones, 2012; Lake Vostok Drilling Project, 2014). Palaeotemperatures within the ice-free areas were derived from Schmittner et al. (2011) which were  $\sim 20\text{ }^{\circ}\text{C}$  lower during the Last Glacial Maximum than pre-industrial levels. Similar estimates were reported by Otto-Bliesner et al. (2006), Bartlein et al. (2010), and others. This estimation, however, applies specifically to the Last Glacial Maximum, when air temperatures reached their lowest recorded values during the Weichselian glaciation. To account for this, temperatures below  $-11\text{ }^{\circ}\text{C}$  from Schmittner et al. (2011) were slightly reduced by  $1\text{--}4\text{ }^{\circ}\text{C}$  to better align with the modelled mean annual temperatures for the Younger Dryas (Renssen & Isarin 1998), a period with comparatively warmer palaeoclimatic conditions. The adjusted palaeotemperatures from Schmittner et al. (2011) were then applied to ice-free land surfaces. However, detailed temperature data for the marginal zones of the ice sheet remain uncertain. To fill this gap, a simple linear interpolation was used between  $-0.5\text{ }^{\circ}\text{C}$  (under the central ice sheet) and the derived temperatures over adjacent ice-free regions.

Additionally, the 3D thermal modelling roughly accounts for the influence of early Cenozoic continental breakup. Two lithosphere-asthenosphere boundary scenarios were considered: (1) shortly after breakup ( $\sim 55\text{ Ma}$ ) and (2) near the end of Brygge Formation deposition ( $\sim 23\text{ Ma}$ ). These time intervals allow me to simulate the increased geothermal gradient due to continental breakup and subsequent lithosphere cooling throughout the Cenozoic.

For the Cenozoic palaeoclimatic conditions, I assume a gradual decrease in surface temperature from  $19\text{ }^{\circ}\text{C}$  at  $55\text{ Ma}$  to present-day mainland temperatures (e.g., Zachos et al., 2001; Eldrett et al., 2009). In deep-sea areas, temperatures are considered to decline from  $9\text{ }^{\circ}\text{C}$  at  $45\text{ Ma}$  to  $0\text{ }^{\circ}\text{C}$  at the present-day seafloor (e.g., Hansen et al., 2013). Intermediate temperatures between the mainland and the deep sea were derived through interpolation.

The thermal disturbance of the study area is additionally related to the syn-breakup magmatism, including lower-crustal underplating, mid- to upper-crustal dyke intrusions, and surface volcanic activity. While magmatic processes can locally elevate the geothermal gradient, their complexity necessitates more detailed investigation, which falls beyond the scope of this study. Consequently, the effects of syn-breakup magmatism have been largely excluded from the current analysis.

Beyond magmatism, the post-breakup deposition of the Brygge (Eocene–lower Miocene) and Kai-Naust (middle Miocene–Pleistocene) formations (layers 1 and 2, respectively) has been approximately incorporated into the 3D thermal model. This accounts for transient near-surface thermal perturbations caused by post-Paleocene sedimentation.

#### 4.1.2 The thermal modelling workflow

The thermal modelling workflow involves the following three steps:

(1) Steady-state calculation (55 Ma ago): A 3D conductive thermal field was modelled with the lithosphere-asthenosphere boundary ( $1300^{\circ}\text{C}$ ) as the lower thermal boundary and the temperature

at the top of Paleocene deposits (or older rocks where the Paleocene is absent) as the upper thermal boundary. The Brygge and Kai-Naust formations were excluded from the modelling. Pre-breakup porosity of sediments was adjusted for shallower depths by removing post-breakup sediments and correcting for the palaeo-seafloor position.

(2) Transient calculation (55–18 Ma ago): The 3D thermal field was modelled from break-up to the early Miocene, using the previous step's results as the initial temperature condition. The lower thermal boundary was set to the inferred lithosphere-asthenosphere boundary at 23 Ma, while the temperature at the upper thermal boundary was the Brygge Formation top (or older rocks where the Brygge Formation is absent). The Kai-Naust Formation was excluded from the modelling. Porosity was adjusted by removing the Kai-Naust Formation and correcting depths. Only full Brygge Formation thickness was considered, ignoring gradual basin infill.

(3) Transient calculation (18 Ma–present day): The final 3D thermal field was obtained using the previous step's results as the initial temperature distribution. The present-day lithosphere-asthenosphere boundary (1300°C) was the lower thermal boundary, while the temperature at the seafloor (offshore) and Earth's surface (onshore) served as the upper thermal boundary. Porosity was based on present-day depths.

In all steps, upper thermal boundary temperatures varied with time.

## 4.2 Input data and thermal properties

### 4.2.1 Structural data

Bathymetry and topography data for the study area were obtained from the Norwegian Mapping Authority. The sedimentary cover of the used 3D structural model is described in Maystrenko et al. (2018).

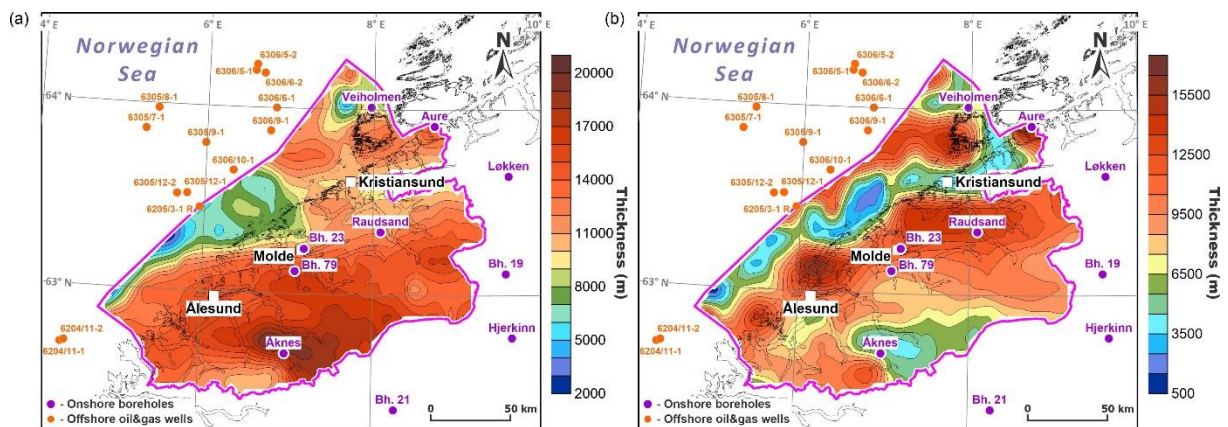


**Figure 14:** Maps showing thicknesses of the upper and middle crustal layers: (a) the upper crust (layer 10 in Table 3); (b) the middle crust (layer 11 in Table 3).

The configuration of the crystalline crust was derived from integrated 3D density and magnetic modelling (Maystrenko et al., 2018). This modelling incorporated the most recent geophysical datasets, primarily deep seismic profiles (Mjelde et al., 1997, 2001, 2002, 2003, 2005, 2009; Raum et al., 2000, 2002, 2006; Breivik et al., 2006, 2009, 2011; Kvarven et al., 2014), along with structural data from Maystrenko & Scheck-Wenderoth (2009), Ebbing & Olesen (2010), Nirrengarten et al. (2014), & Gernigon et al. (2015). The crystalline basement is relatively complex in the offshore areas, where it is overlain by thick sedimentary rocks, whereas the mainland is characterized by mostly exposed crystalline rocks. The uppermost crystalline layers are represented by the upper

and middle crustal layers (Fig. 14a, b). The upper crustal layer varies in thickness, ranging from less than 8 km offshore to ~20 km in southeastern Møre & Romsdal County (Fig. 14a). The middle crustal layer displays a more complex structural pattern, with localized thinning (less than 5 km) and thickening (more than 15 km) (Fig. 14b). The base of the crystalline crust, the Moho topography, is deeply located beneath the Norwegian mainland, contrasting with a much shallower position beneath the Mid-Norwegian continental margin and the oceanic domain.

#### 4.2.2 Thermal properties

**Table 3:** Thermal properties of the layers of the 3D thermal model. Lithology of sediments has been taken from Bell et al. (2014) and NOD (2024).

No	Layer of the 3D structural model	Dominant lithology	Specific heat capacity $C_p$ [J/kgK]	Thermal conductivity of the matrix $k_r$ [W/mK]	Radiogenic heat production $S$ [ $\mu$ W/m <sup>3</sup> ]
1	Kai and Naust (middle Miocene-Pleistocene)	92% shale, 8% sandstone	1180	2.3	0.5-1.5
2	Brygge (Eocene-lower Miocene)	98% shale, 2% sandstone	1180	2.2	0.47-1.5
3	Paleocene	80% shale, 20% sandstone	1180	3.0	0.6-1.39
4	Oceanic layer 2AB	Basalts and tuffs	880	1.8	0.4
5	Upper Cretaceous	95% shale, 5% sandstone	1180	2.5	0.7-1.68
6	Lower Cretaceous	92% shale, 3% sandstone,	1180	2.4	0.81-1.83
7	Pre-Cretaceous	80% shale, 20% sandstone	1180	3.3	0.8-1.64
8	Upper-crustal high-density crystalline	gabbro to anorthositic rocks, metamorphic	880	2.9	0.4
9	Low-density upper-crustal body	metasediments or granite	880	3.0	0.4-2.2
10	Upper-crustal regional layer	granite and gneiss	880	3.2	1.5 (0.9-2.5)
11	Middle crust	granitoids and/or gneiss	950	3.1	0.9 (0.4-2.5)
12	Lower crust	metamorphic rocks	1050	3.0	0.32
13	High-density intracrustal layer	mafic granulites, gabbros	1050	3.0	0.32
14	High-density Lower-crustal layer	gabbros, high-grade metamorphic rocks	1100	2.8 and 3.2	0.2
15	Lithospheric upper mantle	peridotite	1200	4.79	0.03

Before conducting the 3D thermal modelling, thermal properties were assigned to each layer of the 3D structural model, as detailed in Table 3.

Thermal conductivities for sedimentary rocks were derived from estimates, made for the northern Viking Graben (Brigaud et al. 1992), the Mid-Norwegian margin (Eldholm et al. 2005; Pascal 2015), and the Vøring Basin (Midttømme et al. 1995). These were cross-validated with (1) North Sea borehole measurements (Evans 1977), (2) lab data for similar lithologies (Čermak & Rybach 1982; Clauser 2011), and (3) literature reviews (Midttømme & Roaldset 1999). Basalts (Layer 5) were assigned 1.8 W/mK based on Faroe Islands data (Balling et al. 2006). Upper crustal thermal conductivities are based on the lab measurements (Olesen et al. 1993; Slagstad et al. 2009). Deeper crust/mantle values came from published sources (Čermak & Rybach 1982; Hofmeister 1999; Scheck-Wenderoth & Maystrenko 2013).

Thermal conductivities were set as temperature-dependent to account for porosity reduction with depth. For the upper crust, empirical Equation (2) from Sass et al. (1992) has been used.

$$k(T) = k_0 / (1.007 + T(0.036 - 0.0072/k_0)) \quad (2)$$

where  $k(T)$  is the thermal conductivity at temperature  $T$  [W/m·K],  $k_0$  is the thermal conductivity at 0°C [W/m·K],  $T$  is the temperature [°C].

For deeper crust (>300°C), empirical Equation (3) from Vosteen & Schellschmidt (2003) has been applied.

$$k(T) = k_0 / (0.99 + T(a - b/k_0)) \quad (3)$$

where  $k(T)$  is the thermal conductivity at temperature  $T$  [W/m·K],  $k_0$  is the thermal conductivity at 0°C (273.15 K) [W/m·K],  $T$  is the absolute temperature [K]. The constants  $a$  and  $b$  are defined as:  $a = 0.0030 \pm 0.0015$  and  $b = 0.0042 \pm 0.0006$ .

Mantle conductivities used Hofmeister (1999)'s pressure- and temperature-dependent equations (4 and 5).

$$k(T,P) = k_r(298/T)^a \exp[-(4\gamma + 1/3)\alpha(T - 298)](1 + K'_0 P/K_0) + k_{rad} \quad (4)$$

$$k_{rad} = 4.7(0.01753 - 0.00010365T + 2.2451T^2/10^7 - 3.407T^3/10^{11}) \quad (5)$$

where the thermal conductivity  $k(T,P)$  [W/m·K] is a function of temperature  $T$  [K] and pressure  $P$  [Pa]. Here,  $k_r$  represents the thermal conductivity [W/m·K] at room temperature,  $\gamma$  is the Grüneisen parameter (typically  $\gamma = 1$  to 1.4), and  $\alpha$  is a phonon fitting parameter (ranging from 0.25 to 0.45). The term  $\alpha$  denotes the volumetric thermal expansion coefficient as a function of temperature. The bulk modulus  $K_0$  is given as 261 GPa, with its pressure derivative  $K'_0 = 5$ . Additionally,  $k_{rad}$  accounts for the radiative component of thermal conductivity, enhanced as described by van den Berg et al. (2001).

The porosity of sedimentary rocks has been assigned to decrease with depth via exponential density functions (Maystrenko et al., 2018). Fluid thermal conductivity followed water properties (Wagner & Kretzschmar 2008). For details, please see Maystrenko & Gernigon (2018). Heat capacities have been taken to be constant (Table 3), derived from Clauser (2011).

To determine the radiogenic heat production of sedimentary rocks and upper crustal crystalline rocks, natural gamma-ray logs were used. The radiogenic heat production in the selected boreholes was calculated using the empirical relationship between total natural gamma-ray intensity and radiogenic heat production (Equation 6) established by Bückner & Rybach (1996).

$$S = 0.0158 (GR - 0.8) \quad (6)$$

where  $S$  is the radiogenic heat production ( $\mu\text{W}/\text{m}^3$ ) and  $GR$  is the total gamma-ray intensity (API units).

Radiogenic heat production values for the lower crust and lithospheric mantle have been taken to be constant (Table 3). Since predicting radiogenic element content in deep crustal layers lacks

precise mathematical methods. The radiogenic heat production typically decreases with depth and, therefore, constant average values were adopted based on published data for assumed lithological compositions (Čermak & Rybach 1982b; Scheck-Wenderoth & Maystrenko 2008; Vila et al. 2010; Hasterok et al., 2017).

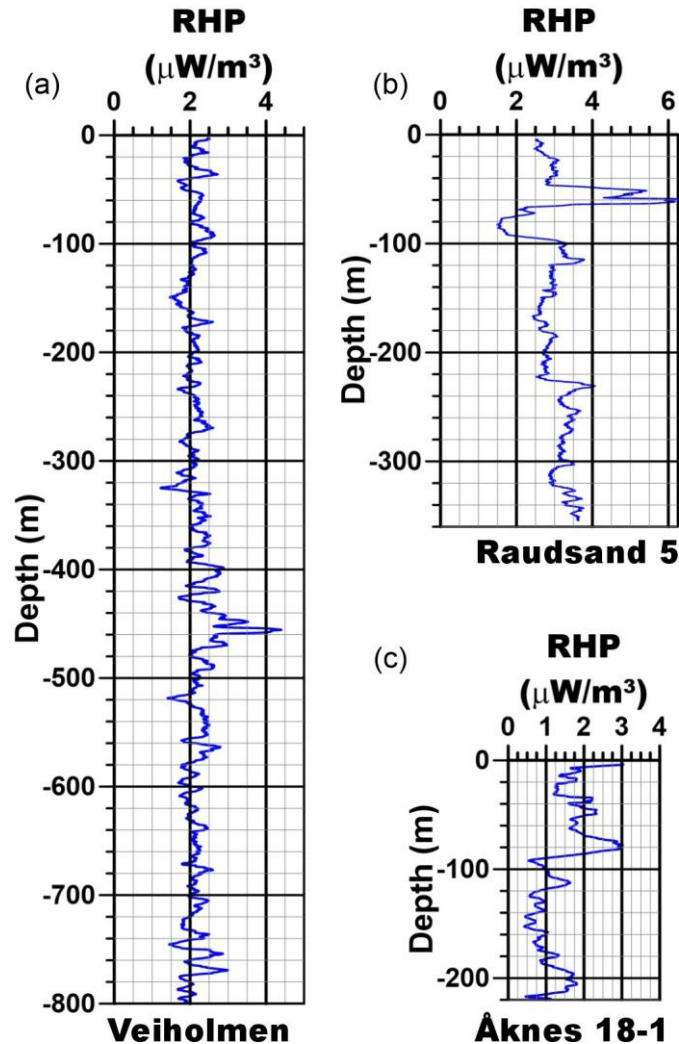


**Figure 15:** Plots display the calculated radiogenic heat production using running-mean averages at 5 m depth intervals. The radiogenic heat production values for the Veiholmen (a) and Raudsand 5 (b) boreholes were derived from natural gamma spectrometry (Maystrenko et al., 2021), while those for the Åknes 18-1 borehole were obtained from natural gamma-ray logs (Elvebakk and Pless, 2018).

Natural gamma logs are available for onshore boreholes logged by NGU. To assess the potential range of radiogenic heat production in the upper crust of Møre & Romsdal County, natural gamma logs and natural gamma spectrometry from the Åknes, Raudsand, and Veiholmen boreholes were used to calculate radiogenic heat production according to Equation 6. The calculation results for these boreholes are presented in Figure 15. The Veiholmen borehole has an average radiogenic heat production of  $2.2 \mu\text{W}/\text{m}^3$ , which has been applied to most of the Møre & Romsdal upper crust (Fig. 16a). In contrast, the Raudsand boreholes show higher radiogenic heat production values. However, since these boreholes are shallower than the Veiholmen one, using their average values (around  $3 \mu\text{W}/\text{m}^3$ ) for the entire upper crust would be problematic. Instead, a lower value of  $2.5 \mu\text{W}/\text{m}^3$  has been assigned to the area surrounding the Raudsand boreholes to account for the elevated radioactive element content in the uppermost crystalline rocks drilled there (Fig. 16a). The

Åknes boreholes, being less than 200 m deep, are not representative of the entire upper crust but still serve as a useful check on the probability of  $2.2 \mu\text{W}/\text{m}^3$  value, derived from the Veiholmen borehole. While the upper crust lithology in the Veiholmen borehole may differ from other parts of the study area, this value effectively aligns the modelled and measured temperatures in the Veiholmen borehole. Due to the lack of other deep data for the mainland, the Veiholmen-derived value remains the preferable estimate.

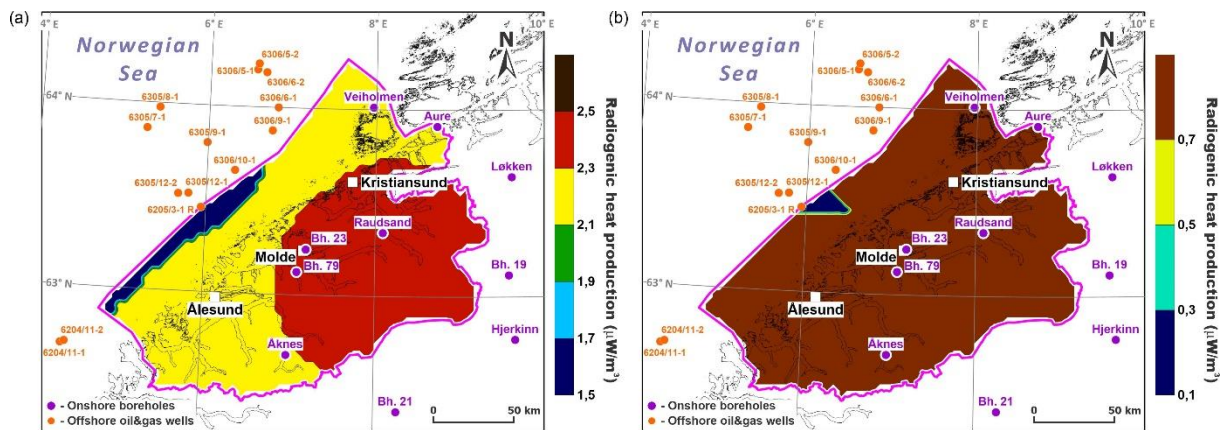


**Figure 16:** Maps showing the assigned radiogenic heat production values for the upper and middle crustal layers: (a) the upper crust and (b) the middle crust.

The upper-crustal regional layer (Layer 10) displays a relatively simple distribution of radiogenic heat production values (Fig. 16a). An area of elevated heat production has been defined near the Raudsand boreholes, while a linear zone of reduced heat production has been included along the coast off Molde and Ålesund (Fig. 16a). This adjustment corresponds to a region where the upper crust undergoes significant thinning (Fig. 14a) and can partially consist of lower-crustal rocks, which typically contain fewer radioactive elements than upper-crustal crystalline material.

In the middle crust (Fig. 16b), radiogenic heat production is nearly uniform at  $0.9 \mu\text{W}/\text{m}^3$  across most of Møre & Romsdal County, except for an offshore zone of lower heat production near Molde, where the middle crust is notably thin and the lower crustal rocks can be present there (Fig. 14b). These values reflect the expected decrease in radioactive element concentrations with depth in the crystalline crust.

### 4.3 Results of the 3D thermal modelling

During the 3D thermal modelling process, the 3D structural data was successfully transformed into a consistent 3D thermal model. The results provide insights into the present-day temperature distribution beneath the Earth's surface in Møre & Romsdal County (Fig. 17). Figure 17 illustrates the subsurface temperature patterns at six selected depths below sea level within the upper part of the 3D thermal model.

Figure 17 reveals a distinct zone of reduced modelled temperatures near the coastline of Møre & Romsdal County, observable across all depth levels. This “cooling” pattern is particularly prominent at shallower depths of 1, 2, and 3 km (Figs. 17a–c). It is still clearly visible at deeper levels (4, 5, and 6 km) where the temperature contrast is slightly less pronounced (Figs. 17d–f). One of the contributing factors to this low thermal anomaly is the thinning of the upper and middle crust in that area (cf. Figs. 14 and 17). However, this is not the only single explanation. Another key factor, amplifying this “cooling” effect, is the high topographic relief, particularly, in the southeastern part of Møre & Romsdal, where mountain elevations exceed 1 km (Fig. 4). It is important to note that the depths referenced in Figure 17 are measured below sea level. Consequently, in areas with high

topography, the true vertical distance from the Earth’s surface to a given depth interval equals the depth below sea level plus the elevation of the overlying terrain. As a result, the southeastern portion of Møre & Romsdal effectively lies 800–1000 m deeper than coastal areas at the same nominal depth below the Earth’s surface. This topographic variation means that if the inland relief were smoother, the temperature distribution would also appear more uniform. Moreover, a part of this low thermal anomaly coincides with regions where the water depth ranges from 50 to 200 meters, further enhancing the temperature contrast in relation to the elevated terrain of the mainland.

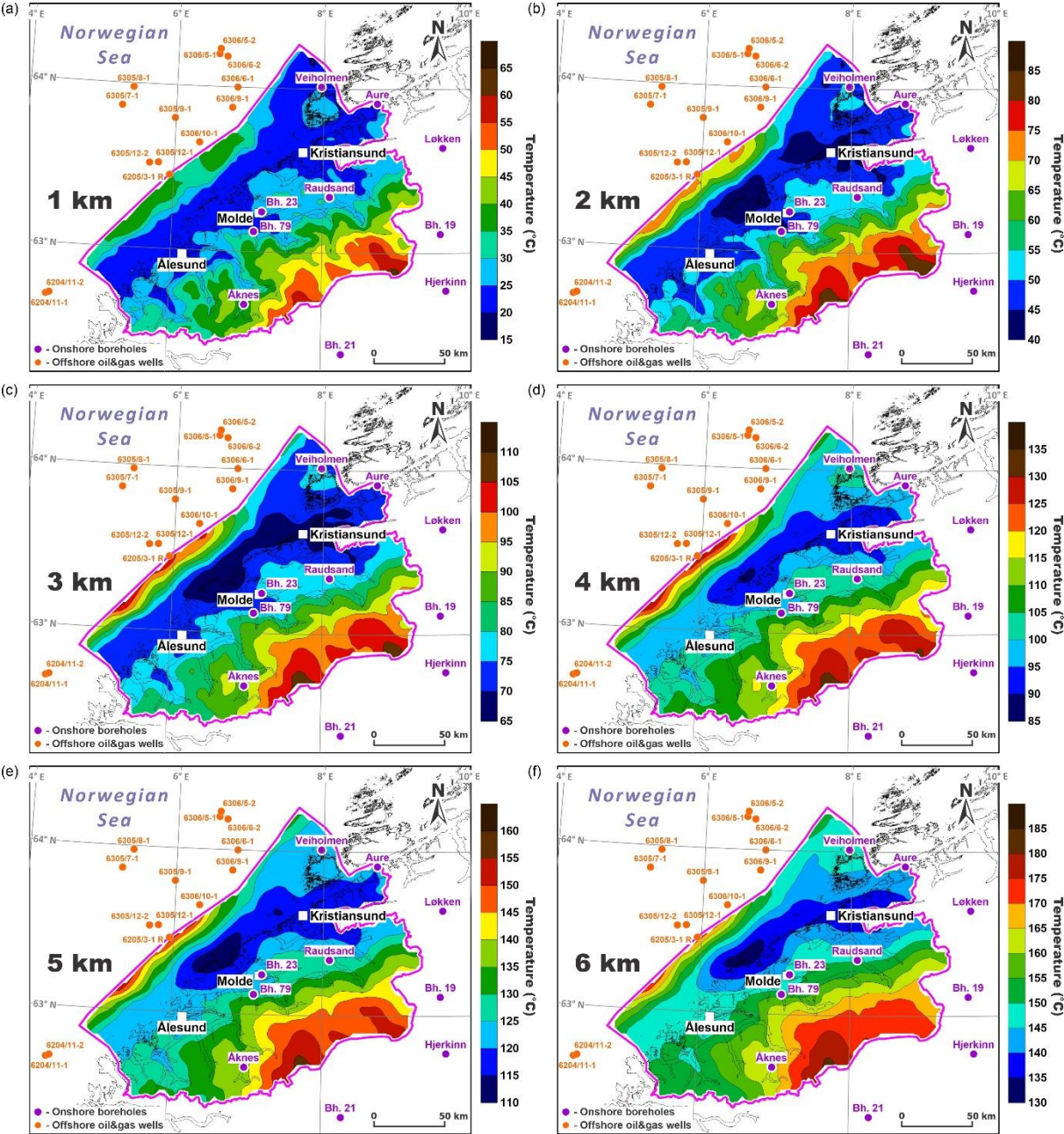


**Figure 17:** Maps showing the modelled temperatures within the uppermost part of Møre & Romsdal County represented by the horizontal slices 3D thermal model for the depths of 1 km (a), 2 km (b), 3 km (c), 4 km (d), 5 km (e) and 6 km (f). The depths are below sea level.

An offshore band of elevated temperatures along the northwestern boundary of Møre & Romsdal is primarily attributed to the thermal blanketing effect of low-conductivity sedimentary rocks. Additional contributions come from crustal thinning and a shallower lithosphere-asthenosphere boundary in that region. Nevertheless, the dominant factor in generating this high thermal anomaly is the insulating effect of the sedimentary cover, which becomes particularly pronounced where the thickness of sediments increases (cf. Figs. 7 and 17).

Therefore, the interaction of crustal structure, bathymetry/topography, and sediment insulation collectively shapes the region's subsurface thermal regime, with each factor leaving a distinct imprint on the observed temperature patterns. The effect of lithospheric thinning is also present, though it appears smoothed due to the study area's relatively small size, comparable to the distance from sea level to the base of the lithosphere.

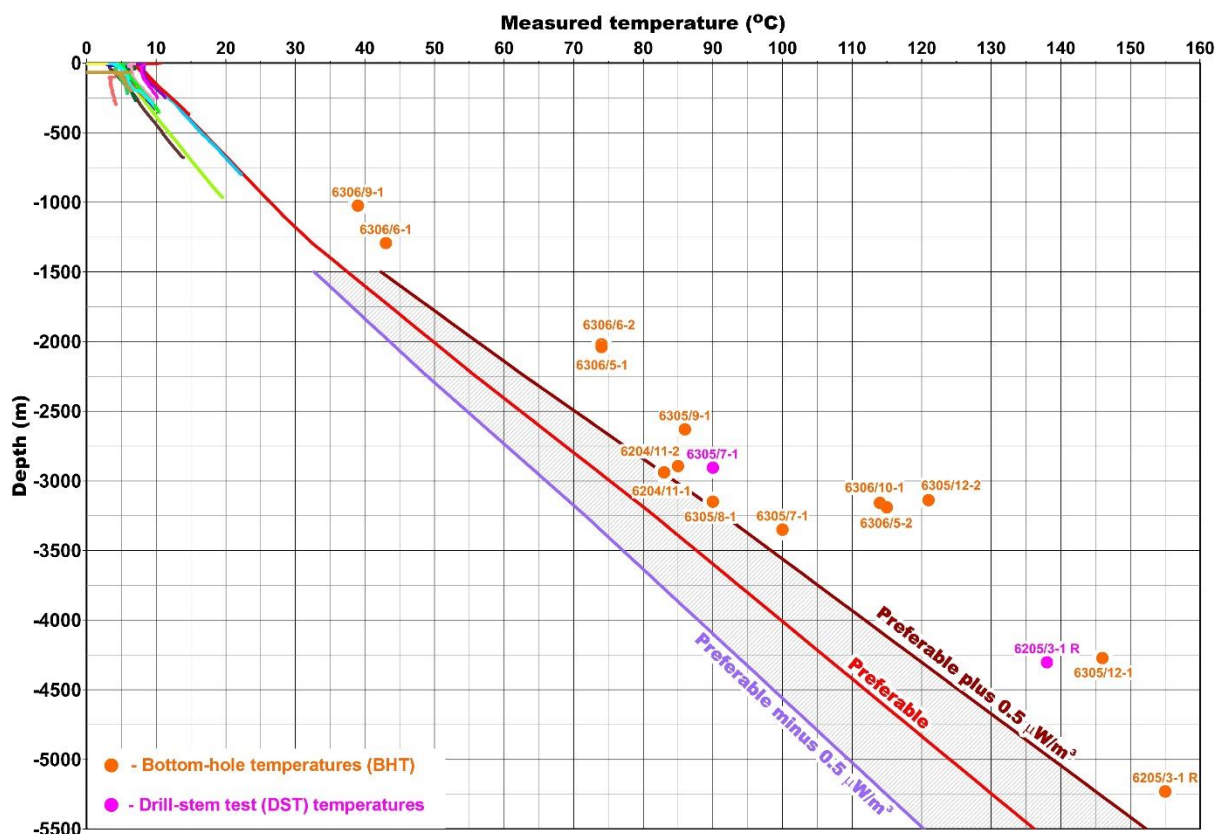


**Figure 18:** Plot showing a comparison of measured temperatures from selected onshore boreholes and offshore wells with modelled temperatures for the hypothetical deep borehole in Molde. The preferred modelled temperature-depth profile is indicated in red. The reddish-brown line represents a scenario with  $0.5 \mu\text{W}/\text{m}^3$  higher radiogenic heat production in the upper and middle crust, while the bluish-violet line corresponds to a  $0.5 \mu\text{W}/\text{m}^3$  lower radiogenic heat production in these layers.

In addition to the temperature maps presented in Figure 17, Figure 18 shows the temperature profile for a hypothetical 5.5-km-deep borehole in Molde. The preferred temperature curve corresponds to the thermal pattern displayed on the temperature maps in Figure 17. Furthermore, the graphs include modelled temperatures for two alternative scenarios: one with reduced radiogenic heat production and another with increased heat production in the upper and middle crustal layers. These cases illustrate potential deviations in subsurface temperature predictions, highlighting the uncertainty in thermal modelling at greater depths. The uncertainty range widens progressively with depth, starting at approximately  $10^\circ\text{C}$  at 1.5 km and reaching slightly more than  $30^\circ\text{C}$  at 5.5 km. This trend reflects the diminishing availability of reliable constraints as depth increases, leading to greater variability in temperature estimates.

Thus, the impact of radiogenic heat production in the middle-upper crystalline crust, which governs temperature pattern, has been evaluated, enabling an estimation of the first-order uncertainty in the modelled temperatures. Sensitivity analysis results in Figure 18 reveal that temperatures at 5.5 km depth can range from approximately 120°C to slightly over 150°C, with the most probable value being around 136°C (Table 4).

**Table 4:** The predicted temperatures for a conceptual 5.5 km deep borehole in Molde.

Scenario with 0.5 $\mu\text{W}/\text{m}^3$ lower radiogenic heat production, °C	Preferable scenario, °C	Scenario with 0.5 $\mu\text{W}/\text{m}^3$ higher radiogenic heat production, °C	Depth below sea level, m
32,7	37,5	42,3	1500
38,1	43,7	49,2	1750
43,6	49,8	56,1	2000
49,0	56,0	63,0	2250
54,7	62,4	70,2	2500
60,3	68,8	77,3	2750
66,0	75,2	84,5	3000
71,7	81,6	91,6	3250
77,1	87,6	98,4	3500
82,5	93,7	105,1	3750
87,9	99,8	111,8	4000
93,3	105,8	118,6	4250
98,7	111,9	125,3	4500
104,1	118,0	132,1	4750
109,5	124,1	138,8	5000
114,9	130,1	145,5	5250
120,3	136,2	152,3	5500

## 5. DISCUSSION

### 5.1 Constraints problems and limitations of the methodology

The main uncertainties affecting the results of the 3D thermal modelling are the following: (1) 3D model resolution (vertical/horizontal), (2) thermal properties of deep layers, (3) heat advection by fluid flow (groundwater flow), (4) palaeoclimatic scenario, (5) lower thermal boundary condition and (8) thermal effect of erosion on the mainland.

The modelled temperatures clearly depend on layer geometry, thermal properties, and the resolution of the input structural data. A key problem of the present 3D thermal modelling is related to the resolution of the structural model, which was originally designed for a regional-scale study of the Mid-Norwegian continental margin rather than the adjacent Norwegian mainland. As a result, the upper crustal layer in Møre & Romsdal County was not properly subdivided into local compositional blocks. Only a rough approximation of radiogenic heat production was applied by dividing the upper crust into three broad units (Fig. 16a). A more accurate representation would require subdividing the upper crust into smaller, geologically constrained blocks based on surface geology and airborne radiometry data. The geometries of these blocks could be further refined using magnetic and gravity datasets. However, due to time constraints, the analysis was completed in just over one month, this level of detail was not incorporated. An additional limitation is associated with the horizontal resolution of the input grids, which were subsequently converted into a low-

resolution mesh with 4 km horizontal cell size. This coarse resolution fails to adequately capture the steep topographic gradients, characteristic for the Møre & Romsdal region. The vertical resolution is more detailed, but it can still be improved by incorporating additional layers of the crystalline crust. While inherent 3D modelling limitations exist, they have been reduced using new borehole data onshore.

The assigned values of the thermal properties of rocks in the deeper sections of the 3D model are not well-constrained, meaning that the adopted values (Table 3) may vary within a plausible range, leading to some deviations in the modelled temperatures.

Conductive heat transfer has been considered as the dominant heat transfer mechanism during the 3D thermal modelling. However, onshore borehole data provide direct evidence of groundwater flow in the uppermost crust of Møre & Romsdal County (Fig. 8). While no data are available on deeper groundwater flow, its presence cannot be excluded and its thermal effect should be explored, particularly, in the areas with steep topographic gradients and fractured crystalline rocks. Moreover, the thermal effect of post-Paleocene deposition has been approximately evaluated, but the simultaneous erosion over the mainland has not been included in the 3D modelling workflow. Incorporating this effect into the modelling would require additional data to constrain erosional rates in both time and space. Uplift and subsequent erosion can elevate isotherms in the upper crust, generating a transient positive thermal anomaly beneath eroded regions. However, palaeo- and present-day groundwater flow may significantly dampen this thermal signal (e.g., Maystrenko et al., 2015), particularly during Quaternary ice sheet melting, when enhanced fluid flow could further reduce the erosion-related thermal influence.

Palaeoclimatic reconstructions play a key role in determining the uppermost thermal regime of the study area. However, these reconstructions inherently carry multiple uncertainties, such as incomplete proxy data, temporal resolution limitations, and interpretive ambiguities, which can affect the accuracy of the 3D thermal modelling results. Addressing these uncertainties is necessary to improve the reliability of the model's predictions.

Additional uncertainties remain regarding the depth of the lithosphere-asthenosphere boundary, which serves as the lower thermal boundary of the model. Maystrenko et al. (2014) examined the thermal effects of the lithosphere-asthenosphere boundary depth variations by comparing two scenarios: a  $\pm 20$  km deviation from the reference depth of 120 km for the base of the lithosphere. Their findings indicate that a 20 km deeper lithosphere-asthenosphere boundary results in a  $\sim 4\%$  temperature variation at 6 km depth, whereas a 20 km shallower lithosphere-asthenosphere boundary leads to a more pronounced  $\sim 12\%$  difference. This suggests that the impact of the lower thermal boundary at shallower depths is higher since the distance between the lower and upper boundaries decreases.

Future improvements could include higher horizontal resolution, more lithological layers, and coupled fluid-flow and heat-transfer simulations. The possible fluid flows require better hydrogeological, lithological, and structural constraints. A more detailed palaeoclimatic scenario would also help to improve the resulting output distribution of temperatures. Therefore, a 3D modelling of coupled groundwater flow and heat transfer incorporating groundwater flow could improve the results, but such an approach would require additional input data and more time to conduct the study.

## **5.2 Implication of the results to deep geothermal potential**

Møre & Romsdal County currently faces an energy deficit, which could be at least partially mitigated using deep geothermal energy. The findings of this study indicate that the most promising areas for high subsurface temperatures are located offshore, where temperatures at a depth of 5 km can reach nearly  $150^{\circ}\text{C}$  which is already sufficient for electricity generation.

In contrast, the mainland areas at similar depth levels exhibit lower temperatures, making them less suitable for power generation since water-based geothermal systems typically require temperatures higher than  $150^{\circ}\text{C}$  for efficient electricity generation. However, theoretical studies

suggest that CO<sub>2</sub> could serve as an efficient working fluid for power generation in deep geothermal systems with temperatures below the typical 150°C threshold, as CO<sub>2</sub>-based systems can operate at lower temperatures (as low as 70–100°C). Nevertheless, deep geothermal energy extraction remains feasible on the mainland through alternative approaches: (1) direct heat extraction from great depths for district heating or industrial applications and (2) heat pump-assisted heat extraction from shallower geothermal reservoirs. The extracted heat can be used to warm buildings. However, transporting heat over long distances is inefficient, meaning deep geothermal boreholes intended solely for heat extraction must be located near the buildings they supply. In contrast, electricity generated from geothermal sources can be transmitted over long distances, even from offshore sites to the mainland.

Offshore areas are particularly promising because existing oil and gas platforms could be converted into deep geothermal power plants with some additional investment, though costs should be assessed beforehand. Since electricity can be transported efficiently over long distances, even remotely located oil and gas platforms could be repurposed for offshore power generation, supplying clean energy to the mainland.

The three largest urban centers in Møre & Romsdal, Molde, Ålesund, and Kristiansund, are all situated along the coast, positioning them as possible candidates for deep geothermal drilling. The current thermal model indicates only minor variations (5–7°C differences) among these locations, which is still within the range of the modelling uncertainties. As a result, there is insufficient data to prioritize one site over another at this stage. To refine these assessments, a new, high-resolution 3D thermal model of Møre & Romsdal County is required. Such a model would provide more precise temperature distribution within the subsurface, enabling better decision-making regarding optimal drilling locations and energy extraction methods. Further exploration, including geophysical modelling, drilling and more detailed 3D thermal numerical modelling, could help validate the presented findings and unlock the details of the region's geothermal potential.

The possible deep groundwater flow in Møre & Romsdal could represent an additional advantage for geothermal energy extraction, since circulating fluids may advectively transport heat from deeper reservoirs toward shallower levels. Such a mechanism could enhance heat transfer and improve the efficiency of geothermal systems. However, the current understanding of deep groundwater flow patterns in the region remains uncertain, making it difficult to assess the extent of this effect. Further hydrogeological studies would be necessary to evaluate the role of deep fluid circulation in the area's geothermal potential.

The deep geothermal boreholes can also serve as thermal storage during peak hydropower generation, particularly when energy consumption is lower than production. This scenario may occur after extended periods of rain when water reservoirs risk overflowing.

## 6. CONCLUSIONS

The analysis of temperature measurements from deep onshore boreholes and offshore hydrocarbon wells (Figs. 5 and 6) indicates that the highest deep geothermal potential is found within offshore areas. This observation is further supported by the results of 3D thermal modelling (Figs. 17 and 18), which indicates elevated subsurface temperatures in the offshore sedimentary basin compared to the mainland regions. Additionally, a clear trend of increasing temperature at equivalent depths from the Earth's surface is observed when moving from inland areas toward the coast (Fig. 5). Based on these findings, the most promising location for a deep geothermal site in Møre & Romsdal would be near the coast or, optimally, offshore on the existing hydrocarbon platforms, where more favorable geothermal conditions are expected (Fig. 19).

The preference for a near-coastal or offshore geothermal site is not only supported by temperature data and the 3D thermal modelling but also by logistical considerations. The region's major population centers, including Ålesund, Molde, and Kristiansund, are all situated along the coastline, ensuring proximity to potential end-users of geothermal energy. Furthermore, existing offshore

infrastructure, such as hydrocarbon platforms, could help the development of geothermal systems by providing ready-made access points to deep, high-temperature reservoirs.

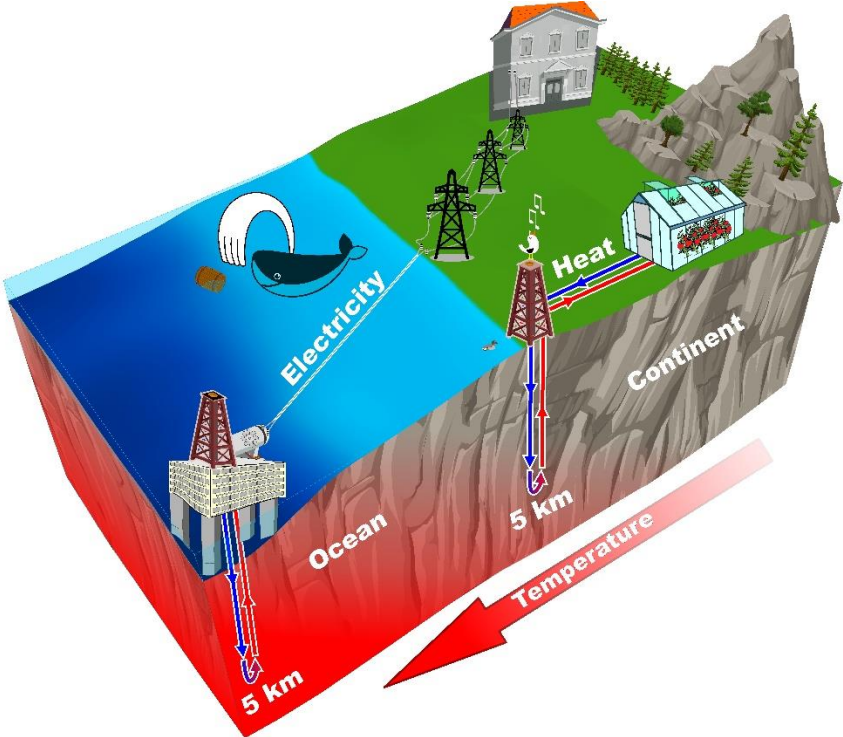


**Figure 19:** Sketch showing potential methods for extracting deep geothermal energy at the continental-oceanic transition zone in the Møre & Romsdal region.

Modelled temperature projections for a hypothetical deep geothermal site in Molde provide additional insights into the geothermal gradient of the region. At a depth of 5 km, the predicted temperature is 124°C (±15°C), while at 4 km, it decreases to 100°C (±12°C), and at 3 km, it reaches 75°C (±9°C). These values align well with expectations for near-coastal transition zones between the mainland and deep offshore sedimentary basins. The uncertainty ranges further strengthen the reliability of these estimates, suggesting that the region holds viable potential for deep geothermal exploitation. Further refinement of the 3D thermal model, supported by newly acquired geophysical data and new geological maps, could improve the precision of deep geothermal resource assessments and provide stronger support for future deep geothermal drilling in the region.

In summary, the integration of direct temperature measurements, 3D thermal modelling, and logistical advantages strongly supports the prioritization of near-coastal or offshore locations for future geothermal development in Møre & Romsdal. Further deep geothermal exploration and targeted drilling in these areas could help confirm and optimize the utilization of this renewable energy resource. By investing in deep geothermal energy production, Møre & Romsdal County could move closer to energy self-sufficiency, contributing to Norway's transition towards sustainable and renewable energy sources.

## REFERENCES

- Andersen, B.G. & Borns Jr., H.W. 1994: *The Ice Age World*. Scandinavian University Press (Universitetsforlaget AS), Oslo. 208 pp.
- Balling, N. & Breiner, C. 2005: Temperature logging by University of Aarhus 2005. in Olesen et al. KONTIKI final report, continental crust and heat generation in 3D. NGU Report no. 2007.042, 63-76.
- Balling, N. 2024: Thermal structure of two deep boreholes in the Siljan Ring, Central Sweden, and palaeoclimatic implications. *Tectonophysics*, 872, 230149. doi:<https://doi.org/10.1016/j.tecto.2023.230149>
- Balling, N., Breiner, N. & Waagstein, R. 2006: Thermal structure of the deep Lopra-1/1A borehole in the Faroe Islands. *Geological Survey of Denmark and Greenland Bulletin* 9, 91–107.
- Bartlein, P.J., Anderson, K.H., Anderson, P.M., Edwards, M.E., Mock, C.J., Thompson, R.S., Webb, R.S., Webb III T. & Whitlock, C. 1998: Palaeoclimate simulations for North America over the past 21,000 years: Features of the simulated climate and comparisons with palaeoenvironmental data. *Quaternary Science Reviews* 17, 549-585.
- Bell, R.E., Jackson, C.A-L., Elliott, G.M., Gawthorpe, R.L., Sharp, I.R. & Michelsen, L. 2014: Insights into the development of major rift-related unconformities from geologically constrained subsidence modelling: Halten Terrace, offshore mid Norway. *Basin Research* 26, 203–224, doi: 10.1111/bre.12049.
- Breivik, A.J., Faleide, J.I., Mjelde, R. & Flueh, R. 2009: Magma productivity and early seafloor spreading rate correlation on the northern Vøring Margin, Norway - Constraints on mantle melting. *Tectonophysics* 468, 206-223.
- Breivik, A.J., Mjelde, R., Faleide, J.I. & Murai, Y. 2006: Rates of continental breakup magmatism and seafloor spreading in the Norway Basin – Iceland plume interaction. *Journal of Geophysical Research* 111, B07102, doi:10.1029/2005JB004004.
- Breivik, A.J., Mjelde, R., Raum, T., Faleide, J.I., Murai, Y. & Flueh, E.R. 2011: Crustal structure beneath the Trøndelag Platform and adjacent areas of the mid-Norwegian margin, as derived from wide-angle seismic and potential field data. *Norwegian Journal of Geology* 90, 141–161.
- Brigaud, F., Vasseur, G. & Caillet, G. 1992: Thermal state in the north Viking Graben (North Sea) determined from oil exploration well data. *Geophysics* 18, 69-88.
- Bücker, C. & Rybach L. 1996: A simple method to determine heat production from gamma-ray logs. *Marine and Petroleum Geology* 13, 373-375.
- Čermak, V. & Rybach, L. 1982: Thermal properties: Thermal conductivity and specific heat of minerals and rocks, in *New Series, Geophysics and space research* 305–343, ed. Angenheister, G., Landolt-Börnstein, Volume 1, subvolume A: Berlin, Springer.
- Clauser, C. 2011: Thermal storage and transport properties of rocks, In: Gupta, H. (ed.), *Heat capacity and latent heat, Encyclopedia of Solid Earth's Geophysics*, 2nd ed. Vol. 2, 1423-1431.
- Ebbing, J. & Olesen, O. 2010: New compilation of basement and basement thickness for the Norwegian continental shelf reveals the segmentation of the passive margin system. In: Vining, B.A. & Pickering, S.C. (eds.) *Petroleum Geology: From mature basins to new frontiers*. Proceedings of the 7th Petroleum Geology Conference. *Petroleum Geology Conference Series* 7, Geological Society of London, 885-897.
- Eldholm, O., Thiede, J. & Shipboard Scientific Party 2005: Thermal conductivity of ODP Hole 104-642C. PANGAEA, doi:10.1594/PANGAEA.79172.
- Eldrett, J.S., Greenwood, D.R., Harding, I.C. & Huber, M. 2009: Increased seasonality through the Eocene to Oligocene transition in northern high latitudes. *Nature* 459, 969–973, doi:10.1038/nature08069.

Elvebakk, H. & Lutro, O. 2017: Logging av fem borehull ved Raudsand, Nesset kommune, Møre og Romsdal. NGU Rapport 2017.020.

Elvebakk, H. & Pless, G. 2018: Borehullslogging Åknes, Stranda kommune, 2017 – 2018. NGU rapport 2018.026.

Elvebakk, H. 2019: Geophysical logging of Veiholmen and Rausand drillholes in Olesen et al. Coop Phase 3 Crustal Onshore-Offshore Project. NGU Report 2019.036, 63-88.

Evans, T.R. 1977: Thermal properties of North Sea rocks. *The Log Analyst* 8, 3-12.

Friðleifsson, G.Ó., Elders, W.A., Zierenberg, R.A., Fowler, A.P.G., Weisenberger, T.B., Mesfin, K.G., Sigurðsson, Ó., et al. 2020: The Iceland Deep Drilling Project at Reykjanes: Drilling into the root zone of a black smoker analog. *Journal of Volcanology and Geothermal Research*, 391, 106435. doi:<https://doi.org/10.1016/j.jvolgeores.2018.08.013>

Gernigon, L., Blichke, A., Nasuti, A. & Sand, M. 2015: Conjugate volcanic rifted margins, seafloor spreading, and microcontinent: Insights from new high-resolution aeromagnetic surveys in the Norway Basin. *Tectonics* 34, 907–933.

Global Volcanism Program, 2024: [Database] Volcanoes of the World (v. 5.2.7; 21 Feb 2025). Distributed by Smithsonian Institution, compiled by Venzke, E. <https://doi.org/10.5479/si.GVP.VOTW5-2024.5.2>

GRANADA - National Groundwater Database 2025: [https://geo.ngu.no/kart/granada\\_mobil/](https://geo.ngu.no/kart/granada_mobil/)

Hansen, J., Sato, M., Russell, G. & Kharecha, P. 2013: Climate sensitivity, sea level, and atmospheric carbon dioxide, *Phil. Trans. Roy. Soc.* A371, 20120284.

Hasterok, D., Gard, M. & Webb, J., 2018: On the radiogenic heat production of metamorphic, igneous, and sedimentary rocks. *Geoscience Frontiers*, 9, 1777–1794. doi:<https://doi.org/10.1016/j.gsf.2017.10.012>

Heikkinen, P., Giese, R., Kueck, J., Kukkonen, I., & Malin, P. 2021: Basement-EGS structure from VSP, drilling, well logs, and geology in Espoo, Finland. In *Using the Earth to Save the Earth - 2021 Geothermal Rising Conference, GRC 2021* (pp. 1519-1530). (Transactions - Geothermal Resources Council; Vol. 45). Geothermal Resources Council.

Hofmeister, A.M. 1999: Mantle values of thermal conductivity and the geotherm from phonon lifetimes. *Science* 283, 1699-1706.

Hokstad, K. & Tanavasuu-Milkeviciene, K. 2017: Temperature prediction by multigeophysical inversion: application to the IDDP-2 well at Reykjanes, Iceland Geotherm Resource Council 41, 1141-52.

<http://dx.doi.org/10.1016/j.tecto.2014.03.021>.

ICES 2012: Factors affecting the distribution of North Sea fish, [http://www.google.no/url?sa=t&rct=j&q=&esrc=s&source=web&cd=1&cad=rja&ved=0CGIQFjAA&url=http%3A%2F%2Fwww.ices.dk%2Fmarineworld%2Ffishmap%2Fpdfs%2Ffactors.pdf&ei=5xwyUOPvJ5KN4gSI\\_YGwAQ&usq=AFQjCNFP7NOM](http://www.google.no/url?sa=t&rct=j&q=&esrc=s&source=web&cd=1&cad=rja&ved=0CGIQFjAA&url=http%3A%2F%2Fwww.ices.dk%2Fmarineworld%2Ffishmap%2Fpdfs%2Ffactors.pdf&ei=5xwyUOPvJ5KN4gSI_YGwAQ&usq=AFQjCNFP7NOM).

Jones, N. 2012: Russians celebrate Vostok victory. Team finally drills into biggest Antarctic subglacial lake. *Nature* 482, 287, doi:10.1038/482287a.

Korablev, A., Smirnov, A. & Baranova, O.K. 2014: Climatological Atlas of the Nordic Seas and Northern North Atlantic. In: D. Seidov, A. R. Parsons, (eds.) NOAA Atlas NESDIS 77, 122 pp., doi: 10.7289/V54B2Z78.

Kukkonen, I.T. & Pentti, M. 2021: St1 Deep Heat Project: Geothermal energy to the district heating network in Espoo. *IOP Conference Series: Earth and Environmental Science*, 703, 012035, IOP Publishing. doi:10.1088/1755-1315/703/1/012035

- Kvarven, T., Ebbing, J., Mjelde, R., Faleide, J.I., Libak, A., Thybo, H., Flueh, E.R. & Murai, Y. 2014: Crustal structure across the land-ocean transition off Møre, mid-Norway, from wide-angle seismic and gravity data. *Tectonophysics* 626, 21-40.
- Lake Vostok Drilling Project, 2014: <http://www.southpolestation.com/trivia/10s/lakevostok.html>
- Maystrenko, Y., Scheck-Wenderoth, M. 2009: Density contrasts in the upper mantle and lower crust across the continent–ocean transition: constraints from 3-D gravity modelling at the Norwegian margin. *Geophysical Journal International* 179, 536-548. doi: 10.1111/j.1365-246X.2009.04273.x.
- Maystrenko, Y.P. & Gernigon, L. 2018: 3D temperature distribution beneath the Mid-Norwegian continental margin (the Vøring and Møre basins). *Geophysical Journal International*, 212 (1), 694–724, doi: 10.1093/gji/ggx377.
- Maystrenko, Y.P. 2019: 3D Thermal model of the Frøya High. In Olesen et al., Coop Phase 3 Crustal Onshore-Offshore Project, NGU Report no. 2019.036, 205-247.
- Maystrenko, Y.P., Olesen, O. & Elvebakk, H.K. 2015a Indication of deep groundwater flow through the crystalline rocks of southern Norway. *Geology* 43(4), 327-330, doi: 10.1130/G36318.1.
- Maystrenko, Y.P., Elvebakk, H.K., Osinska, M., Olesen, O. 2021: New heat flow data from the Veiholmen and Raudsand boreholes, middle Norway. *Geothermics* 89, 101964, doi: 10.1016/j.geothermics.2020.101964.
- Maystrenko, Y.P., Gernigon, L., Nasuti, A. & Olesen, O. 2018: Deep structure of the Mid-Norwegian continental margin (the Vøring and Møre basins) according to 3D density and magnetic modelling. *Geophysical Journal International*, 212 (3), 1696–1721, doi: 10.1093/gji/ggx491.
- Midttømme, K. & Roaldset, E. 1999: Thermal conductivity of sedimentary rocks: uncertainties in measurement and modelling. Geological Society, London, Special Publications 158, 45-60.
- Midttømme, K., Slættem, J., Roaldset, E. & Zielinski, G.W. 1995: Thermal conductivity of unconsolidated marine sediments from Vøring Basin, Norwegian Sea. SAGE 57th Conference and Technical Exhibition - Glasgow, Scotland.
- Mjelde, R., Digranes, P., van Schaack, M., Shimamura, H., Shiobara, H., Kodaira, S. & Næss, O. 2001: Crustal structure of the outer Vøring Plateau, offshore Norway, from ocean bottom seismic and gravity data, *Journal of Geophysical Research* 106, 6769–6791.
- Mjelde, R., Kasahara, J., Shimamura, H., Kamimura, A., Kanazawa, T., Kodaira, S., Raum, T. & Shiobara, H. 2002: Lower-crustal seismic velocity-anomalies; magmatic underplating or serpentinized peridotite? Evidence from the Voring Margin, NE Atlantic, *Mar. Geophys. Res.* 23, 169–183.
- Mjelde, R., Kodaira, S. & Sellevoll, M.A. 1997: Crustal structure of the central part of the Voring Basin, mid-Norway margin, from ocean bottom seismographs, *Tectonophysics* 277, 235–257.
- Mjelde, R., Raum, T., Kandilarov, A., Murai, Y. & Takanami, T. 2009: Crustal structure and evolution of the outer Møre Margin, NE Atlantic, *Tectonophysics* 468, 224–243.
- Mjelde, R., Raum, T., Myhren, B., Shimamura, H., Murai, Y., Takanami, T., Karpuz, R. & Næss, U. 2005: Continent-ocean transition on the Voring Plateau, NE Atlantic, derived from densely sampled ocean bottom seismometer data, *Journal of Geophysical Research* 110, B05101, 1–19.
- Mjelde, R., Raum, T.A.B., Shimamura, H., Murai, Y., Takanami, T. & Faleide, J.I. 2005: Crustal structure of the Vøring margin, NE Atlantic: a review of geological implications based on recent OBS-data. In: Doré, A.G. & Vining, B.A. (eds.). *North-West European Petroleum Geology and Global Perspectives: Proceedings of the 6th Conference*. Geological Society of London, 803-813.

- Mjelde, R., Shimamura, H., Kanazawa, T., Kodaira, S., Raum, T. & Shiobara, H. 2003: Crustal lineaments, distribution of lower-crustal intrusives and structural evolution of the Voring Margin, NE Atlantic; new insight from wide-angle seismic models, *Tectonophysics* 369, 199–218.
- Nirrengarten, M., Gernigon, L. & Manatschal, G. 2014: Lower-crustal bodies in the Møre volcanic rifted margin: Geophysical determination and geological implications. *Tectonophysics* 636 143–157.
- NOD 2024: <https://factpages.sodir.no/en/wellbore/PageView/Exploration/All>
- Olesen, O., Reitan, M. & Sæther, P.O. 1993: Petrofysisk Database PETBASE 3.0, Brukerbeskrivelse, NGU Internrapport 93.023, Trondheim, Norway.
- Olsen, L., Sveian, H., Bergstrøm, B., Ottesen, D. and Rise, L., 2013: Quaternary glaciations and their variations in Norway and on the Norwegian continental shelf. In Olsen, L., Fredin, O. and Olesen, O. (eds.) *Quaternary Geology of Norway*, Geological Survey of Norway, Special Publication 13, 27–78.
- Ottersen, G. 2009: A digital temperature archive for the Norwegian Sea. Institute of marine research, Bergen, Norway, 38 pp.
- Otto-Bliesner, B.L., Brady, E. Clauzet, G. Tomas, R., Levis, S. & Kothavala, Z. 2006: Last glacial maximum and Holocene climate in CCSM3. *J. Climate* 19, 2526-2544.
- Pascal, C. 2015: Heat flow of Norway and its continental shelf. *Marine and Petroleum Geology* 66, 956-969.
- Pattyn, F. 2010: Antarctic subglacial conditions inferred from a hybrid ice sheet/ice stream model, *Earth's Planet. Sci. Lett.* 295, 451-461.
- Popov, V.S. & Kremenetskii, A.A. 1999: Deep and superdeep scientific drilling on continents, *Soros Educational Journal: Sciences about Earth*, 11, 61-68.
- Popov, Y.A., Pevzner, S.L., Pimenov, V.P. & Romushkevich, R.A., 1999: New geothermal data from the Kola superdeep well SG-3. *Tectonophysics*, 306, 345–366.  
doi:[https://doi.org/10.1016/S0040-1951\(99\)00065-7](https://doi.org/10.1016/S0040-1951(99)00065-7)
- Price, P.B., Nagornov, O.V., Bay, R., Chirkin, D., He, Y., Miocinovic, P., Richards, A., Woschnagg, K., Koci, B. & Zagorodnov V. 2002: Temperature profile for glacial ice at the South Pole: implications for life in a nearby subglacial lake. *Proceedings National Academy of Sciences USA* 99, 7844-7847.
- Raum, T. 2000: Crustal structure and evolution of the Faeroe, Møre and Vøring margins from wide-angle seismic and gravity data, Dr. thesis. University of Bergen, Bergen, Norway.
- Raum, T., Mjelde, R., Digranes, P., Shimamura, H., Shiobara, K.S., Haatvedt, G., Sorenes, N. & Thorbjørnsen, T. 2002: Crustal structure of the southern part of the Voring Basin, mid-Norway margin, from wide-angle seismic and gravity data, *Tectonophysics* 355, 99–126.
- Raum, T., Mjelde, R., Shimamura, H., Murai, Y., Bråstein, E., Karpuz, R.M., Kravik, K. & Kolstø, H.J. 2006: Crustal structure and evolution of the southern Vøring Basin and Vøring Transform Margin, NE Atlantic, *Tectonophysics* 415, 167–202.
- Renssen, H. & Isarin, R.F.B. 1998: Surface temperature in NW Europe during the Younger Dryas: AGCM simulation compared with temperature reconstructions. *Climate Dynamics* 14, 33-44.
- Rønning, J. S., Elvebakk, H., Lutro, O., Dagestad, A. og Jæger, Ø. 2018: Grunnundersøkelser ved Raudsand, Nesset kommune i Møre og Romsdal. Tolking av borehullslogging og vannanalyser. NGU Rapport 2018.024.
- Sass, J. H., Lachenbruch, A. H., Moses, T. H., Jr. & Morgan, T. 1992: Heat flow from a scientific research well at Cajon Pass, California. *Journal of Geophysical Research* 97(B4), 5017–5030.

- Scheck-Wenderoth, M. & Maystrenko, Y.P. 2013: Deep control on shallow heat in sedimentary basins. *Energy Procedia* 40, 266-275, doi.org/10.1016/j.egypro.2013.08.031.
- Schmittner, A., Urban, N.M., Shakun, J.D., Mahowald, N.M., Clark, P.U., Bartlein, P.J., Mix, A.C. & Rosell-Mele, A. 2011: Climate Sensitivity Estimated from Temperature Reconstructions of the Last Glacial Maximum. *Science* 334, 1385-1388, doi: <http://dx.doi.org/10.1126/science.1203513>
- Seifu, A. 2004: Evaluation of recent temperature and pressure data from wells in Tendaho geothermal field, Ethiopia and from well HG-1 at Hágöngur, Iceland. Report 15, 325-348.
- Siegert, M.J., Dowdeswell, J.A., Hald, M. & Svendsen, J.I.. 2001: Modelling the Eurasian ice sheet through a full (Weichselian) glacial cycle. *Global and Planetary Change* 31, 367-385.
- Slagstad, T., Balling, N., Elvebakk, H., Midttømme, K., Olesen, O., Olsen, O. & Pascal, C. 2009: Heat-flow measurements in Late Palaeoproterozoic to Permian geological provinces in south and central Norway and a new heat-flow map of Fennoscandia and the Norwegian–Greenland Sea. *Tectonophysics* 473, 341–361.
- Steinberger, B. & Becker, T.W. 2018: A comparison of lithospheric thickness models. *Tectonophysics*, 746, 325–338. doi:<https://doi.org/10.1016/j.tecto.2016.08.001>
- Turcotte, D.L. & Schubert, G. 2002: *Geodynamics*, Cambridge University Press : Cambridge, United Kingdom.
- Tveito, O.E., Førland, E., Heino, R., Hanssen-Bauer, I., Alexandersson, H., Dahlström, B., Drebs, A., Kern-Hansen, C., Jónsson, T., Vaarby Laursen, E. & Westman, Y. 2000: Nordic temperature maps. DNMI-Report 09/00 KLIMA, 54 pp.
- van den Berg, A.P., Yuen, D.A. & Steinbach, V. 2001: The effects of variable thermal conductivity on mantle heat-transfer. *Geophys. Res. Lett.* 28, 875-878.
- Vilà, M., Fernández, M. & Jiménez-Munt, I. 2010: Radiogenic heat production variability of some common lithological groups and its significance to lithospheric thermal modeling. *Tectonophysics* 490, 152–164.
- Vosteen, H.-D. & Schellschmidt, R. 2003: Influence of temperature on thermal conductivity, thermal capacity, and thermal diffusivity for different types of rock. *Physics and Chemistry of the Earth* 28, 499–509.
- Wagner, W. & Kretzschmar, H.-J. 2008: *International steam tables – properties of water and steam based on the Industrial Formulation IAPWS-IF97*. Springer-Verlag, Berlin.
- Zachos, J., Pagani, M., Sloan, L., Thomas, E. & Billups, K. 2001: Trends, rhythms, and aberrations in global climate 65 Ma to present. *Science* 292(5517), 686–693.



GEOLOGICAL  
SURVEY OF  
NORWAY

· NGU ·

Geological Survey of Norway  
PO Box 6315, Sluppen  
N-7491 Trondheim, Norway

Visitor address  
Leiv Eirikssons vei 39  
7040 Trondheim

Tel (+ 47) 73 90 40 00  
E-mail [ngu@ngu.no](mailto:ngu@ngu.no)  
Web [www.ngu.no/en-gb/](http://www.ngu.no/en-gb/)